A New Model of the Dynamics of the Flow in a Thermosyphon

By Elizabeth Burroughs, Evangelos Coutsias, Louis Romero

(Received 27 December 2003)

Using the Navier-Stokes equations to model the flow in a thermosyphon, one arrives at a sequence of bifurcation problems. We have derived a model where, in the case of a circular loop, the first Fourier modes exactly decouple from all other Fourier modes, leaving a system of three coupled nonlinear PDEs that completely describe the flow in the thermosyphon. We have characterized the flow through two bifurcations, identifying periodic solutions for flows of Prandtl number greater than 19, a much lower value than predicted previously. Because of the quadratic nonlinearity in this system of equations, it is possible to find the global stability limit, and we have proved it is identical to the first bifurcation point.

The numerical study of the model equations is based on a highly accurate Fourier-Chebyshev spectral method, combined with asymptotic analysis at the various bifurcation points. Three-dimensional computations with a FEM CFD code (MPSalsa), are also pursued. All three approaches are in close agreement.

1. Introduction

When a closed vertical loop of fluid is heated from below, a sequence of bifurcations ensues, leading from pure conduction, to a convective unidirectional flow, to periodic or chaotic flow. This is the problem of convection in a closed-loop thermosyphon, also called a natural convection loop. This problem has implications for hydrothermal circulation in the earth's crust Torrance(1979), as well as engineering relevance for the performance of heating/cooling systems Japikse(1973). Moreover, it offers useful insights into general convective phenomena. The problem is appealing because of the possibility of observing complicated behavior in a physically simple system.

Pioneering work in this field was done by Keller(1966) and Welander(1967) who identified that unsteady flow results directly from the dynamics of the system, rather than from an unsteady force. Recent mathematical models by Velázquez(1994) and Rodríguez-Bernal & Van Vleck(1998) focus on the transition to complex dynamics. These works have modeled viscous and inertial terms with friction factors, leading to predictions of complex dynamical behavior in qualitative agreement with observations. Also, recent work by Yuen & Bau(1996) has used feedback to control the onset of chaos.

The approach taken in our work is to derive a reduced system of PDEs describing convection in a slender hoop. We apply techniques of asymptotic analysis in combination with highly accurate spectral numerical methods to analyze this system, derived from the Navier-Stokes equations in the Boussinesq approximation by averaging around the loop. Validation of the predictions of the reduced model requires comparison with numerical simulations of the full, 3-dimensional system, and the code MPSalsa Salinger *et al.*(1999), Salinger *et al.*(1996), Shadid *et al.*(1999), developed at Sandia National Laboratories to compute solutions to reacting flow problems on massively parallel computers, is used

to carry out such comparisons. Good agreement is found between asymptotic analysis, simulations of the reduced model and three-dimensional FEM calculations, in the ranges where the latter are feasible.

Under our main assumption, the mean radius of curvature of the loop is supposed to be large compared to the radius of a cross-section of the tube. Then centrifugal effects can be ignored, so that the shape of the loop enters only via the gravity function. The equations that result are equivalent to those where the flow takes place in a straight tube where gravity acts as a function of axial distance along the tube. In the case where the shape of the loop is circular the first Fourier modes exactly decouple from all other Fourier modes, leaving a system of three coupled nonlinear PDEs that completely describe the flow in the thermosyphon. This is in contrast to existing models, which use truncations, adjustable parameters, and other simplifications that are avoided in the present formulation.

Two dimensionless parameters characterize the process, the Grashof number Gr (2.17), which is proportional to the thermal gradient Θ and the Prandtl number Pr (2.15) which is a property of the material, the ratio of kinematic viscosity ν to thermometric conductivity κ. Linearizing about the numerically computed purely conducting trivial state, one arrives at an eigenvalue problem from which convection is found to onset as a pitchfork bifurcation at a critical value of the Grashof number, Gr_p. This value is independent of the Prandtl number. Using energy methods, we formulate a variational problem that proves that the trivial solution is globally stable for $Gr < Gr_p$. We use continuation in Grashof number to numerically follow the convecting branch and also linearize the flow about the numerically computed convective state to determine the onset of a Hopf bifurcation at a second critical value, $Gr_h > Gr_p$. The location of this bifurcation and its character is shown to be dependent on Pr. By numerically estimating the coefficients of a Landau equation describing the weakly nonlinear evolution of perturbations about the convective state near the Hopf bifurcation point we show that the bifurcation is subcritical for Prandtl numbers less than ≈ 19 and supercritical for Prandtl numbers greater than ≈ 19. For comparison we mention that the Prandtl numbers for water, alcohol, ??? and glycerine, respectively, are 6.75, 16.6, ??? and 7250, Landau & Lifshitz(1999).

The outline for this paper is as follows. In Section 2, we give a derivation of our PDE model, followed by a further simplification to a Lorenz-like ODE model presented in appendix A. Section 3 analyzes the pitchfork bifurcation in each model and gives a proof of the global stability of the trivial branch up to this first bifurcation point. Section 4 analyzes the Hopf bifurcation. Section 5 tracks the periodic solution in the ODE model and discusses such a tracking in the PDE model. In Section 6 we present the numerical framework that we use in this research. Section 7 summarizes our findings.

2. Problem Formulation

We study flow in a closed loop thermosyphon—a tube which is bent into a vertical closed loop, heated symmetrically from below. The cross-section of the tube and the shape of the loop can be arbitrary. For simplicity, the present formulation will focus on a circular cross-section and a circular loop.

We assume that the radius of the tube is small compared to its length, so that we can think of the flow as if it takes place in a straight tube with gravity a function of the axial distance along the tube. Periodic boundary conditions are imposed on all the model variables (see figure 1).

Begin with the Boussinesq equations

$$\nabla \cdot \mathbf{u} = 0 \tag{2.1}$$

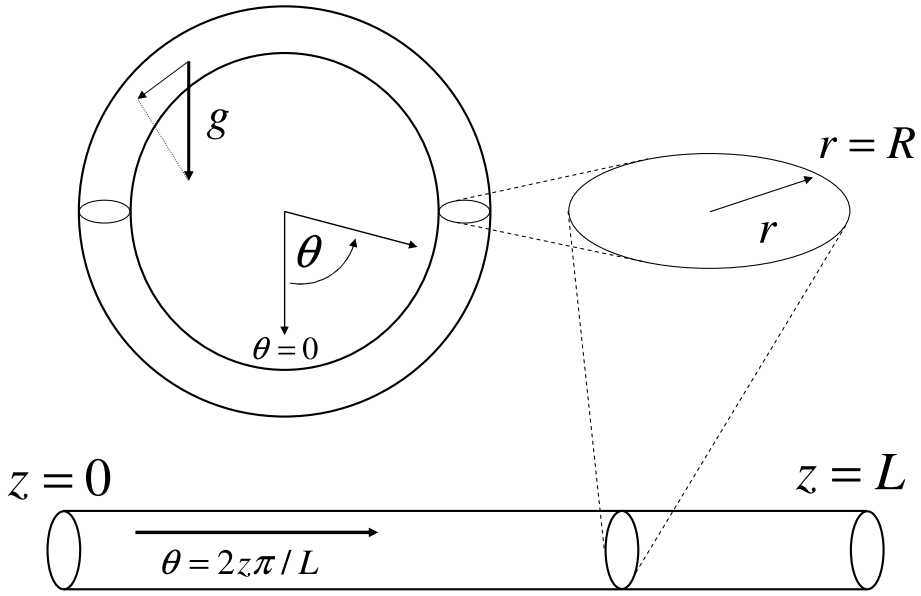

FIGURE 1. Problem geometry

$$\frac{\partial \mathbf{u}}{\partial t} + \mathbf{u} \cdot \nabla \mathbf{u} + \nabla \left(\frac{p}{\rho} \right) = \nu \nabla^2 \mathbf{u} + g\alpha(T - T_0)\mathbf{e}_z \tag{2.2}$$

$$\frac{\partial T}{\partial t} + \mathbf{u} \cdot \nabla T = \kappa \nabla^2 T. \tag{2.3}$$

where $\mathbf{u}$ is velocity, p is pressure, T is temperature, and t is time, and we have the parameters ρ (density), ν (kinematic viscosity), g (gravity), α (thermal expansion), and κ (thermometric conductivity). T_0 is a reference temperature. Then enforcing that the flow has only an axial velocity component and writing the gravity function $f(\frac{2\pi z}{L})$, one arrives at the equations

$$\frac{\partial w}{\partial z} = 0 \tag{2.4}$$

$$\frac{\partial w}{\partial t} + \frac{\partial}{\partial z} \left(\frac{p}{\rho} \right) = \nu \nabla^2 w + \alpha(T - T_0) g f \left(\frac{2\pi z}{L} \right) \tag{2.5}$$

$$\frac{\partial T}{\partial t} + w \frac{\partial T}{\partial z} = \kappa \nabla^2 T \tag{2.6}$$

Here w is axial velocity and z is the axial direction.

The equation of continuity implies that $w = w(x, y, t)$, and so

$$\frac{\partial}{\partial z} \left(\frac{p}{\rho} \right) - \alpha(T - T_0) f(\frac{2\pi z}{L}) = F(x, y, t) \ .$$

Upon integration over the length L of the loop, periodicity of p implies that

$$F(x,y,t) = -\frac{g\alpha}{L}\int_{-L/2}^{L/2}(T(x,y,z,t)-T_0)\,f\left(\frac{2\pi z}{L}\right)dz$$

and we arrive at

$$\frac{\partial w}{\partial t} - \frac{g\alpha}{2\pi}\int_{-\pi}^{\pi}(T(x,y,\theta,t)-T_0)\,f(\theta)d\theta = \nu\nabla^2 w \tag{2.7}$$

$$\frac{\partial T}{\partial t} + \frac{2\pi}{L}w\frac{\partial T}{\partial \theta} = \kappa\left(\nabla^2 T + \frac{4\pi^2}{L^2}\frac{\partial^2 T}{\partial \theta^2}\right). \tag{2.8}$$

Now ∇^2 is the two dimensional (x,y) Laplacian operator and $\theta = \frac{2\pi z}{L}$.

Boundary conditions are

$$T(x,y,\theta,t) = T(x,y,\theta+2\pi,t)$$

$$w(x,y,t) = 0 \;\; on \;\; \partial S$$

$$T(x,y,\theta,t) = T_0 + T_{wall}(\theta) \;\; on \;\; \partial S\,.$$

The following step distinguishes the present model formulation from other models. For a circular loop, set $f(\theta) = \sin\theta$. Introducing $\phi(x,y)$ and $\psi(x,y)$, the mode-1 Fourier sine and cosine coefficients of $T(x,y,\theta,t)$:

$$\phi(x,y) = \frac{1}{2\pi}\int_{-\pi}^{\pi}\sin(\theta)\,(T(x,y,\theta,t)-T_0)\,d\theta$$

$$\psi(x,y) = \frac{1}{2\pi}\int_{-\pi}^{\pi}\cos(\theta)\,(T(x,y,\theta,t)-T_0)\,d\theta$$

and multiplying the heat equation by $\sin\theta$ and $\cos\theta$ respectively and integrating from $-\pi$ to π, find

$$\frac{\partial \phi}{\partial t} - \frac{2\pi}{L}\psi w = \kappa\left(\nabla^2\phi - \frac{4\pi^2}{L^2}\phi\right) \tag{2.9}$$

$$\frac{\partial \psi}{\partial t} + \frac{2\pi}{L}\phi w = \kappa\left(\nabla^2\psi - \frac{4\pi^2}{L^2}\psi\right)\,. \tag{2.10}$$

Notice that these two modes completely decouple from the rest of the Fourier modes. There is no truncation involved, and therefore this formulation is exact for the given loop assumptions.

After integrating, the momentum equation (2.5) is given by:

$$\frac{\partial w}{\partial t} - g\alpha\phi = \nu\nabla^2 w. \tag{2.11}$$

The boundary conditions are

$$w(x,y) = 0 \;\; on \;\; \partial S$$

$$\phi(x,y) = \frac{1}{2\pi}\int_{-\pi}^{\pi}\sin(\theta)T_{wall}(\theta)d\theta = A_0 \text{ on } \partial S$$

$$\psi(x,y) = \frac{1}{2\pi}\int_{-\pi}^{\pi}\cos(\theta)T_{wall}(\theta)d\theta = A_1 \text{ on } \partial S$$

where A_0 and A_1 are the mode-1 Fourier sine and cosine coefficients of $T_{wall}(\theta)$, respectively. Impose that T_{wall} is an even function of θ, so $A_0 = 0$. Then for simplicity drop the subscript, denoting $A_1 = A$.

Define the dimensionless variables by

$$\phi = A\tilde{\phi}$$

$$\psi = A\tilde{\psi}$$

$$w = \frac{g\alpha R^2 A\kappa}{\nu^2}\tilde{w}$$

$$t = \frac{R^2}{\nu}\tilde{t}.$$

$$x = R\tilde{x}$$

$$y = R\tilde{y}\ .$$

Inserting these into equations 2.9 - 2.11 gives:

$$Pr\frac{\partial\tilde{\phi}}{\partial\tilde{t}} - Gr\tilde{\psi}\tilde{w} = \tilde{\nabla}^2\tilde{\phi} - \sigma^2\tilde{\phi} \tag{2.12}$$

$$Pr\frac{\partial\tilde{\psi}}{\partial\tilde{t}} + Gr\tilde{\phi}\tilde{w} = \tilde{\nabla}^2\tilde{\psi} - \sigma^2\tilde{\psi} \tag{2.13}$$

$$\frac{\partial\tilde{w}}{\partial\tilde{t}} - Pr\tilde{\phi} = \tilde{\nabla}^2\tilde{w} \tag{2.14}$$

where the parameters are the diffusion ratio Pr (Prandtl number) (2.15), the aspect ratio σ (2.16), and the control parameter Gr (Grashof number) (2.17):

$$\mathrm{Pr} = \frac{\nu}{\kappa}\ , \tag{2.15}$$

$$\sigma = \frac{2\pi R}{L}\ , \tag{2.16}$$

$$Gr = \frac{\mathcal{R}}{Pr} = \frac{2\pi g\alpha R^4 A}{\nu^2 L} \tag{2.17}$$

where $\mathcal{R}$ is the Rayleigh number. The system given in 2.12—2.14 is the reduced PDE model that is the focus of this study. In appendix A we present a further reduction to an ODE model, the Lorenz system, Lorenz(1963).

3. Stability of the Trivial Solution

Here we provide the analysis of the linear stability of the trivial solution. Expand the system 2.12—2.14 about the steady solution by

$$\begin{pmatrix} \phi \\ \psi \\ w \end{pmatrix} = \begin{pmatrix} \phi_0 \\ \psi_0 \\ w_0 \end{pmatrix} + \epsilon \begin{pmatrix} \phi_1 \\ \psi_1 \\ w_1 \end{pmatrix} + O(\epsilon^2).$$

Consider the expansion in a neighborhood of the critical Grashof number, $Gr = Gr_p$.

The zero order solution is given by

$$\begin{pmatrix} \phi_0 \\ \psi_0 \\ w_0 \end{pmatrix} = \begin{pmatrix} 0 \\ 1 \\ 0 \end{pmatrix}\ .$$

and the first order solution is

$$\begin{pmatrix} \phi_1 \\ \psi_1 \\ w_1 \end{pmatrix} = a_1 \begin{pmatrix} \gamma_{01}^2 J_0(\gamma_{01} r) \\ 0 \\ Pr J_0(\gamma_{01} r) \end{pmatrix}.$$

The critical Grashof number is given by

$$Gr_p = \frac{\gamma_{01}^4}{Pr}$$

Details of the analysis are left to an appendix.

3.1. *Global Stability of the Trivial Branch*

We will analyze the global stability of the trivial solution. There is a limit in the parameters (Grashof number and Prandtl number) below which any perturbation will settle to the trivial solution. This limit is identical to the pitchfork bifurcation point found in appendix B. Because we will show that the trivial branch is globally stable up to the pitchfork bifurcation point, this provides a proof that the pitchfork bifurcation is supercritical, in agreement with the formal perturbation analysis presented in appendix B.

The proof of global stability will proceed as follows. First we will define an energy function that depends on a parameter λ. The rate of change of energy can be maximized by a function $Gr(\lambda)$ of the Grashof number, and each value of λ corresponds to a different energy rate. We will show that this rate of change of energy is always negative. Then maximizing this function of Grashof number over all values of λ, we find the optimal energy function, that is, the one that gives the largest value of Gr for which a decaying energy rate can be guaranteed. This value of Gr is the global stability limit, and corresponds to the pitchfork bifurcation point.

The equations are

$$Pr\phi_t = Grw\psi + \nabla^2\phi \tag{3.1}$$

$$Pr\psi_t = -Grw\phi + \nabla^2\psi \tag{3.2}$$

$$w_t = Pr\phi + \nabla^2 w \tag{3.3}$$

along with boundary conditions

$$\phi(1) = w(1) = 0$$

$$\psi(1) = 1\ .$$

To facilitate the analysis, rescale equations 3.1–3.3 so that the Grashof number appears symmetrically. Define

$$w = \sqrt{Gr}\tilde{w}.$$

Then equations 3.1–3.3 become

$$Pr\phi_t = \sqrt{Gr}\tilde{w}\psi + \nabla^2\phi \tag{3.4}$$

$$Pr\psi_t = -\sqrt{Gr}\tilde{w}\phi + \nabla^2\psi \tag{3.5}$$

$$\tilde{w}_t = \sqrt{Gr}Pr\phi + \nabla^2\tilde{w}. \tag{3.6}$$

For simplicity, we will drop the $\tilde{}$ on the w.

Consider a disturbance $(\hat{\phi}, \hat{\psi}, \hat{w})$ about the base flow (ϕ_0, ψ_0, w_0); for the trivial branch, this base flow is $(0, 1, 0)$, so that

$$(\phi, \psi, w) = (0 + \hat{\phi}, 1 + \hat{\psi}, 0 + \hat{w}).$$

The disturbance to the base flow satisfies:

$$\hat{\phi}_t = \frac{\sqrt{Gr}}{Pr}\hat{w} + \frac{\sqrt{Gr}}{Pr}\hat{w}\hat{\psi} + \nabla^2\hat{\phi}$$
$$\hat{\psi}_t = -\frac{\sqrt{Gr}}{Pr}\hat{w}\hat{\phi} + \nabla^2\hat{\psi}$$
$$\hat{w}_t = \sqrt{Gr}Pr\hat{\phi} + \nabla^2\hat{w}.$$

From here on we drop the hat notation.

Now form a family of energy functions that depend on the parameter λ:

$$\mathcal{E} = \langle\phi^2\rangle + \langle\psi^2\rangle + \lambda\langle w^2\rangle, \tag{3.7}$$

where the $\langle\cdot\rangle$ notation is a volume integral, $\int_V \cdot dV$:

$$\langle\phi_t,\phi\rangle + \langle\psi_t,\psi\rangle + \lambda\langle w_t, w\rangle =$$
$$\frac{\sqrt{Gr}}{Pr}\langle w,\phi\rangle + \lambda\sqrt{Gr}Pr\langle\phi, w\rangle + \frac{1}{Pr}\langle\nabla^2\phi,\phi\rangle + \frac{1}{Pr}\langle\nabla^2\psi,\psi\rangle + \lambda\langle\nabla^2 w, w\rangle.$$

Use Green's identity to rewrite the Laplacian terms, using that the disturbance satisfies null boundary conditions, and the Reynolds transport theorem to rewrite the time derivative terms. This leads to the following theorem:

Theorem 3.1*For equations 3.4–3.6, the energy defined by the family of curves 3.7 satisfies the following equation.*

$$\frac{\partial\mathcal{E}}{\partial t} = \frac{\sqrt{Gr}}{Pr}\left(1+\lambda Pr^2\right)\langle w,\phi\rangle - \frac{1}{Pr}\langle|\nabla\phi|^2\rangle - \frac{1}{Pr}\langle|\nabla\psi|^2\rangle - \lambda\langle|\nabla w|^2\rangle. \tag{3.8}$$

This equation is made up of the energy dissipation terms (the gradient terms) and the energy production terms. We wish to find the balance between dissipation and production terms so that the total rate of change of energy will always be negative, keeping in mind that this equation defines the energy for a family of curves, one for each λ.

First we will show that for each λ there is a maximum Grashof number where this rate of change of energy is always negative. Then we will maximize this over all λ to find the optimal energy function.

Equation 3.8 is of the form

$$\frac{\partial\mathcal{E}}{\partial t} = \int_V \mathcal{F}(r,\mathbf{y},\mathbf{y}')dV \; = J$$

where $\mathbf{y} = (\phi,\psi,w)^T$. Notice that J is a quadratic functional; it is because of this that the following analysis holds.

It is clear that for $Gr = 0$, $\frac{\partial\mathcal{E}}{\partial t}$ is negative, and that for small values of Gr, there is still decay. There is a critical value of Gr where there will cease to be decay; one can employ the Calculus of Variations to calculate this critical value.

First we will formulate the problem as a minimization problem. The critical Gr is bounded above if the ratio of the dissipation to production is bounded below. That is,

$$\sqrt{Gr} < \min\left(\frac{-\frac{1}{Pr}\langle|\nabla\phi|^2\rangle - \frac{1}{Pr}\langle|\nabla\psi|^2\rangle - \lambda\langle|\nabla w|^2\rangle}{\frac{\sqrt{Gr}}{Pr}\left(1+\lambda Pr^2\right)\langle w,\phi\rangle}\right).$$

The "decay constant lemma" proved by Joseph Joseph(1976) guarantees the existence of a lower bound for this ratio.

One can use the Calculus of Variations to solve this minimization problem, and this yields an eigenvalue problem. Taking the first variation of J, one gets

$$\delta J = \int_V (\mathcal{F}_y - \frac{d}{dr}\mathcal{F}_{y'})h(r)dV = 0.$$

The solutions $\mathbf{y}$ satisfy null boundary conditions. Using the Fundamental Lemma of the Calculus of Variations, the Euler-Lagrange equation must be satisfied:

$$\mathcal{F}_y - \frac{d}{dr}\mathcal{F}_{y'} = 0,$$

which is the eigenvalue problem

$$\sqrt{Gr}\left(\frac{1+\lambda Pr^2}{Pr}\right)w + \frac{2}{Pr}\nabla^2\phi = 0$$

$$\frac{2}{Pr}\nabla^2\psi = 0$$

$$\sqrt{Gr}\left(\frac{1+\lambda Pr^2}{Pr}\right)\phi + 2\lambda\nabla^2 w = 0.$$

The equation for ψ decouples and is independent of Gr. Now notice that this is of the same form as the eigenvalue problem solved in the linear stability analysis of the pitchfork bifurcation, equation B 1. The solutions of this eigenvalue problem have the form

$$\begin{pmatrix} \phi \\ w \end{pmatrix} = \begin{pmatrix} c_1 \\ c_2 \end{pmatrix} J_0(\gamma_{m0}r)$$

where $\gamma = \gamma_{0,k}, k = 1, 2, 3, \ldots$ is a zero of the J_0 Bessel function. From $\nabla^2\phi = -\gamma_{0k}^2\phi$ and $\nabla^2 w = -\gamma_{0k}^2 w$ obtain the condition

$$\begin{vmatrix} \frac{-\gamma_{0k}^2}{Pr} & \frac{\sqrt{Gr}}{2Pr}(1+\lambda Pr^2) \\ \left(\frac{\sqrt{Gr}}{2Pr}\right)(1+\lambda Pr^2) & -\lambda\gamma_{0k}^2 \end{vmatrix} = 0.$$

The result is stated as a theorem.

Theorem 3.2 *The critical Gr is given by the following equation.*

$$Gr(\lambda) = \frac{4\lambda\gamma_{0k}^4 Pr}{(1+\lambda Pr^2)^2}$$

Each value of λ corresponds to a Grashof number that is the maximum value for which the energy will always decay. Take the derivative with respect to λ to find the value of λ that maximizes Gr. This is easily seen to be $\lambda = \frac{1}{Pr^2}$, leading to

$$Gr \leq \frac{\gamma_{0k}^4}{Pr}.$$

Depending on the specific root $\gamma_{0,k}$ of J_0, the decay rate has a negative extremum at $Gr = \frac{\gamma_{0k}^4}{Pr}$. However, only the value $k = 1$ corresponds to a maximum, as is shown below.

3.2. *Details of the Maximization*

The first variation has only determined that there is an extremum; it must be shown that there is a maximum. Use the following theorem Gelfand & Fomin(1991):

Theorem 3.3*If $P(x) > 0$ and $[a, b]$ contains no conjugate points to a, then $\int_a^b Ph'^2 + Qh^2 dx$ is positive definite for all $h(x)$ such that $h(a) = h(b) = 0$.*

A conjugate point $\tilde{a}$ to a is defined as a point for which $-\frac{d}{dx}Ph' + Qh = 0$ has a solution that vanishes for $x = a$ and $x = \tilde{a}$ but is not identically 0.

The original formulation is of the form

$$\int_V P\mathbf{y}'^2 + Q\mathbf{y}^2 dV,$$

where $P(x)$ is

$$\text{diag}[\frac{-1}{Pr}, \frac{-1}{Pr}, -\lambda].$$

For the region to contain no conjugate points, choose the first Bessel zero, $s = s_{0,1}$, and then the rate of change of energy, $\frac{\partial \mathcal{E}}{\partial t}$, is negative definite, so the extremum found is a maximum.

The global stability limit for the trivial solution is identical to the linear stability limit for this non-convective branch, which in terms of Ra is

$$Ra_c = \gamma_{01}^4.$$

4. Stability and Bifurcation of the Convective Branch

In this section, we will examine the linear stability of the convective branch and perform a bifurcation analysis of the Hopf bifurcation. We use a weakly nonlinear stability analysis to examine the solution in a neighborhood of a steady state solution. Assuming completeness of the eigenfunctions of the linearized system, a solution can be expanded

$$\mathbf{u}(r, t) = \sum_i \mathbf{A} e^{\lambda_i t} \mathbf{u}(r) + c.c.,$$

where *c.c.* denotes the complex conjugate. The system under consideration in this analysis is 2.12—2.14. Denoting the solution $\mathbf{u} = \begin{pmatrix} \phi \\ \psi \\ w \end{pmatrix}$, write the system as

$$\frac{\partial \mathbf{u}}{\partial t} + L\mathbf{u} = N\mathbf{u}.$$

Let $\hat{L}$ denote the extension of the operator L, interpreted as a distribution, where

$$\langle \hat{L}u, v \rangle = \langle u, L^* v \rangle$$

for all u in L^2 and all test functions v in the domain of L^*. Then one can use Fredholm's Alternative Theorem Keener(1995):

Theorem 4.1*Fredholm's Alternative Theorem*
For the differential operator $\hat{L}$, the solution $\hat{L}u = \hat{f}$ exists if and only if $\langle \hat{f}, v \rangle = 0$ for all v for which $L^* v = 0$.

Additionally, we employ a multiple time-scale analysis, allowing $\tau = \epsilon^2 t$. The slow time scale is suggested by the dependence of the most unstable eigenvalues on Gr in the vicinity of Gr_p. The base state is time independent, and in this analysis one considers perturbations that can depend on the "slow" time, τ.

The goal is to identify the nonlinear behavior of the solution near the bifurcation point.

4.1. *Linear Analysis*

We recscale the time variable so that the bifurcating periodic solution has frequency 1. Then, the bifurcation frequency will enter the system explicitly. To do this we make the substitution $s = \omega t$, and using the notation

$$\mathbf{u} = \begin{pmatrix} \phi \\ \psi \\ w \end{pmatrix}$$

write the system as follows:

$$(\omega D\partial_s - I\nabla^2 - A)\mathbf{u} = GrF(\mathbf{u}),$$

with

$$F(\mathbf{u}) = u_3 M\mathbf{u} = u_3 \begin{bmatrix} 0 & 1 & 0 \\ -1 & 0 & 0 \\ 0 & 0 & 0 \end{bmatrix} \mathbf{u},$$

$$D = \begin{bmatrix} Pr & 0 & 0 \\ 0 & Pr & 0 \\ 0 & 0 & 1 \end{bmatrix},$$

$$A = \begin{bmatrix} 0 & 0 & 0 \\ 0 & 0 & 0 \\ Pr & 0 & 0 \end{bmatrix}.$$

Expand the solution

$$\mathbf{u} = \mathbf{u}_0(r) + \epsilon\mathbf{u}_1(s, r) + O(\epsilon^2).$$

Consider the expansion in a neighborhood of the critical Grashof number, $Gr = Gr_p$. Expand the frequency as

$$\omega = \omega_0 + \epsilon\omega_1 + O(\epsilon^2).$$

This leads to the system

$$\begin{aligned} \left((\omega_0 D\partial_s - I\nabla^2 - A) + \epsilon\omega_1 D\partial_s\right)(\mathbf{u}_0 + \epsilon\mathbf{u}_1) = \\ (u_{3,0} M\mathbf{u}_0 + \epsilon u_{3,0} M\mathbf{u}_0)\epsilon J_0\mathbf{u}_1)\, Gr_h \end{aligned}$$

where the Jacobian is given by

$$J_0 = \begin{bmatrix} 0 & u_{3,0} & u_{2,0} \\ -u_{3,0} & 0 & -u_{1,0} \\ 0 & 0 & 0 \end{bmatrix},$$

and the operators at each order are

$$L_0 = \omega_0 D\partial_s - I\nabla^2 - A$$

$$L_1 = \omega_1 D\partial_s.$$

See the appendix for details. Solutions at each order are computed numerically.

4.2. *A Numerical Scheme to Extract Landau Coefficients*

We can continue this analysis up to order ϵ^3, allowing us to get a characterization of the bifurcation. At this order we arrive at a Landau equation

$$\frac{da(\tau)}{d\tau} = j\alpha a(\tau) + \beta|a(\tau)|^2 a(\tau)$$

. As an alternative to computing the coefficients numerically, we can use the following numerical scheme to extract the Landau coefficients.

It is the signs of the real parts of α and β in the equation that determine whether the bifurcation is sub- or supercritical. Writing $a(\tau) = r(\tau)e^{i\theta(\tau)}$ and α and β as $\alpha_r + i\alpha_i$, $\beta_r + i\beta_i$, respectively, gives

$$\frac{dr}{d\tau} = j\alpha_r r + \beta_r r^3$$

$$\frac{d\theta}{d\tau} = j\alpha_i + \beta_i r^2.$$

Compute the time integration of the full equations, with an initial value of $\mathbf{u}_0 + \epsilon\mathbf{A}_{1i}$, where $\mathbf{u}_0$ is the convective solution at the bifurcation point and $\mathbf{A}_{1i}$ is the imaginary part of the eigenvector associated with the leading eigenvalue at the bifurcation point. Note that this is just a particular choice of constants in the $O(\epsilon)$ solution

$$(c_r + ic_i)e^{i\omega_0 t}(\mathbf{A}_{1r} + i\mathbf{A}_{1i}) + c.c.$$

At every time t, compute the solution $\Phi(r,t)$. The solution must take the form

$$\Phi(r,t,\tau) = \mathbf{u}_0 + \epsilon(a(\tau)(\mathbf{A}_{1r} + i\mathbf{A}_{1i})e^{i\omega_0 t} + c.c.) + \text{ (exponentially decaying modes).}$$

Extract the values $a(\tau)$, given $\mathbf{A}_{1r}$, $\mathbf{A}_{1i}$, and ω_0. In terms of r and θ, this is the equation

$$\frac{\Phi(r,t,\tau) - \mathbf{u}_0}{\epsilon} =$$
$$2((r\cos\theta\mathbf{A}_{1r} - r\sin\theta\mathbf{A}_{1i})\cos(\omega_0 t) - (r\cos\theta\mathbf{A}_{1i} + r\sin\theta\mathbf{A}_{1r})\sin(\omega_0 t)).$$

Integrating $\frac{\Phi-\mathbf{u}_0}{\epsilon}$ over a period against $\cos(\omega_0 t)$ and $\sin(\omega_0 t)$ respectively will yield $2(r\cos\theta\mathbf{A}_{1r} - r\sin\theta\mathbf{A}_{1i})$ and $-2(r\cos\theta\mathbf{A}_{1i} + r\sin\theta\mathbf{A}_{1r})$. Solve this system of two equations in two unknowns to find $r\cos\theta$ and $r\sin\theta$ at each point t_n, $n = 1, 2, 3, \ldots$. Extract $r_n = r(t_i)$ from these and formulate the least squares problem

$$\frac{dr}{d\tau} = j\alpha_r r + \beta_r r^3$$

and solve for the constants α_r and β_r. Approximate

$$\frac{dr}{d\tau}(t_n) = \frac{r(t_{n+1}) - r(t_{n-1})}{\epsilon^2 2\pi/\omega_0} + O(\epsilon^4).$$

(See Bergeron *et al.*(2000) for another discussion of the use of this method of extracting Landau coefficients.)

Simple linear analysis will give an estimate of the coefficient α_r. We will compare this to the one found by the above extraction method as a check of accuracy.

We will now report data obtained on the full PDE system using this method. Results from running this extraction procedure at different Prandtl numbers for various Grashof numbers are given in table 1. Solutions decay for 10 periods before data is collected (the time step used is 10^{-4}) to allow the next most unstable mode to decay. Notice the good agreement between the linear analysis and the extracted linear coefficient α; for the cubic coefficient the equation is scaled so that $\beta \times (Gr_c - Gr)$ should be consistent, and this is the case. (The formula for computing $\frac{dr}{d\tau}$ is second order, explaining the error present in calculating the linear coefficients.)

Figure 2 shows the ratio of $\frac{j\alpha}{\beta}$ for various Prandtl numbers for Gr approximately 2% below Gr_c. From the Hopf bifurcation theorem, when this ratio is positive the bifurcation is subcritical and when it is negative the bifurcation is supercritical. For Pr near 19 the

	Gr	linear α_r	extract α_r	extract β_r
$Pr = 7$	$Gr_h = 351.7679$			
	345.0	-4.80×10^{-4}	-4.80×10^{-4}	0.738×10^{-4}
	341.0	-4.85×10^{-4}	-4.85×10^{-4}	0.457×10^{-4}
$Pr = 15$	$Gr_h = 200.6050$			
	196.0	-6.33×10^{-4}	-6.33×10^{-4}	0.197×10^{-4}
	194.0	-6.36×10^{-4}	-6.36×10^{-4}	0.129×10^{-4}
$Pr = 20$	$Gr_h = 227.9197$			
	223.0	-4.00×10^{-4}	-4.01×10^{-4}	-0.065×10^{-4}
	221.0	-4.02×10^{-4}	-4.02×10^{-4}	-0.045×10^{-4}
	232.8358	3.91×10^{-4}	3.92×10^{-4}	-0.079×10^{-4}
	234.8358	3.90×10^{-4}	3.90×10^{-4}	-0.058×10^{-4}

TABLE 1. Landau coefficients for the PDE system

		N	extract α_r	extract β_r
$Pr = 7$	$Gr = 345$			
		32	-4.80×10^{-4}	0.738×10^{-4}
		64	-4.80×10^{-4}	0.809×10^{-4}
		128	-4.80×10^{-4}	0.702×10^{-4}
$Pr = 15$	$Gr = 196$			
		32	-6.33×10^{-4}	0.197×10^{-4}
		64	-6.33×10^{-4}	0.196×10^{-4}
		128	-6.33×10^{-4}	0.199×10^{-4}
$Pr = 20$	$Gr = 223$			
		32	-4.01×10^{-4}	-0.065×10^{-4}
		64	-4.01×10^{-4}	-0.069×10^{-4}
		128	-4.00×10^{-4}	-0.073×10^{-4}

TABLE 2. Landau coefficients as computed for various mode discretizations N

bifurcation changes criticality from sub- to supercritical. While the Lorenz equations do predict a supercritical Hopf bifurcation, they predict the change at a much higher Prandtl number (on the order of $P = 200$ Note that P=200 corresponds to Pr=??? while P=19 corresponds to ???, and experimental verification is feasible). The difference between the present model and the Lorenz model is significant in this respect.

5. The Supercritical Hopf Bifurcation

This model captures periodic behavior of the flow in the thermosyphon in a parameter value range that is not found in Lorenz-type models, specifically, the change from a

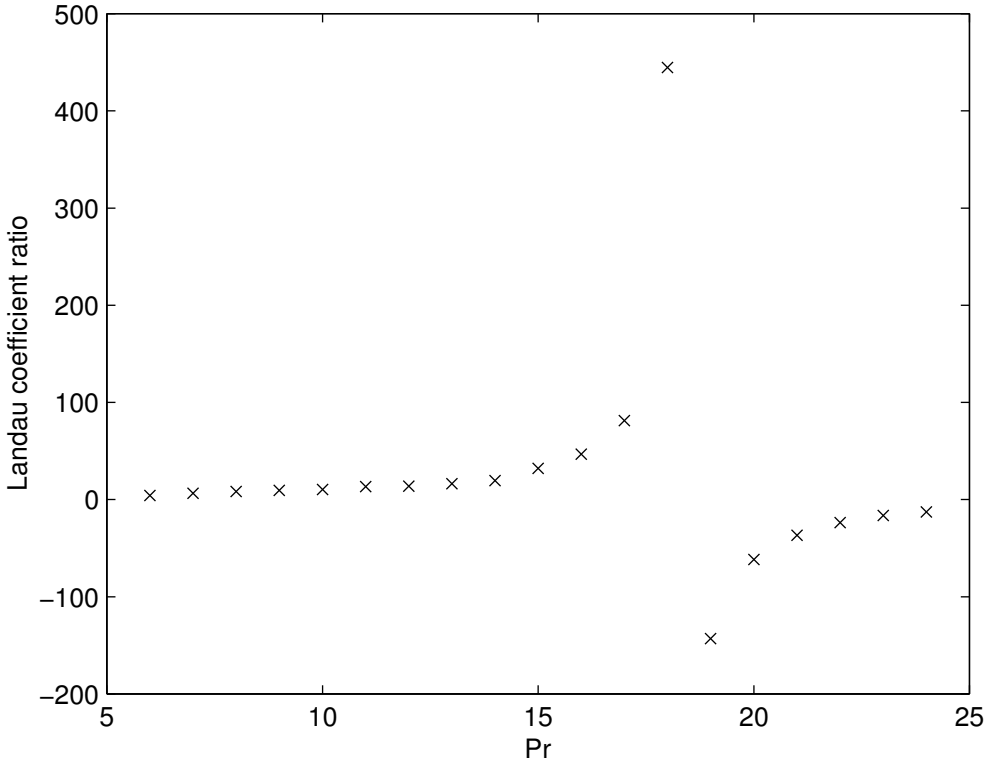

FIGURE 2. The ratio of Landau coefficients for the PDE model indicating the criticality of the Hopf bifurcation

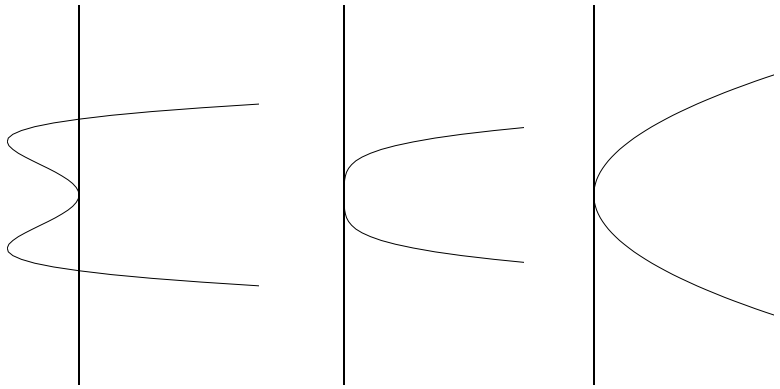

FIGURE 3. Plots of solution vs. Gr_c for $Pr < Pr_c$, $Pr = Pr_c$, $Pr > Pr_c$, respectively.

sub- to supercritical Hopf bifurcation at a Prandtl number of ≈ 19. This is a significant difference between the models and is evidence that, in particular for flows with Pr greater than 19, the reduction to the Lorenz equations is not an accurate model of the flow.

The point (Pr_c, Gr_c) is the most interesting point in parameter space. Here the branching becomes singular, with a Landau equation of the form

$$\frac{da}{d\tau} = \alpha_1 a + \alpha_5 a^5.$$

In the vicinity of this critical point, the equation is of the form

$$\frac{da}{d\tau} = \alpha_1 a + \alpha_3 a^3 + \alpha_5 a^5.$$

where α_3 is very small; this corresponds to the first sketch in figure 3. In the neighborhood of this critical Prandtl number, the bifurcation diagram has a progression similar to that shown in figure 3. For values of Pr just below Pr_c, there is a subcritical bifurcation. This bifurcation must turn around, because of the global stability limit. At Pr_c, the structure is quartic. At $Pr > Pr_c$, the bifurcation is supercritical.

With this result, the opportunities for further research with this model are abundant. The immediate questions that arise are

(a) Expand the solution in the parameter Pr. What is the characterization of the Landau equation governing this change from sub- to supercritical?

(b) Is there chaotic behavior above Pr_c?

(c) Is there periodic behavior below Pr_c?

Answers to these questions will provide more insight into the dynamics of the flow as captured by this model.

6. Numerical Analysis

We numerically compute the solution to the system 2.12–2.14 at given Pr and Gr numbers. The primary method of discretization is the pseudospectral method, briefly described below. More complete discussion can be found, for example, in the works of Gottlieb and Orszag Gottlieb & Orszag(1977), Fornberg Fornberg(1998), and Canuto *et al* Canuto *et al.*(1988).

Following the notation of Gottlieb and Orszag, for each t, $\mathbf{u}(x,t)$ is an element of a Hilbert Space $\mathcal{H}$ with an inner product and a norm. For each $t > 0$, $\mathbf{u}(x,t)$ is a member of the subspace $\mathcal{B}$ of $\mathcal{H}$ where functions in the subspace satisfy the boundary conditions of the problem.

In this work we expand the solution

$$\mathbf{u}(x) = \sum_{m=0}^{M} a_m T_m(x)$$

where

$$T_m(x) = \cos(m \arccos(x))$$

are the Chebyshev functions. One gets the expansion coefficients

$$a_n = \frac{2}{c_n} \int_{-1}^{1} u(x) T_m(x) (1-x)^{-\frac{1}{2}} dx$$

with $c_0 = 2, c_m = 1, m \geq 1$.

The method used here is a spectral collocation (pseudospectral) method. In this method, the expansion functions are not required to satisfy the boundary constraints. Rather, the boundary constraints are imposed as conditions for determining the expansion coefficients. Then make the residual zero at as many spatial points as possible.

This code uses the Gauss-Lobatto points, $x_j = \cos \frac{\pi j}{M}$, and so the Chebyshev expansion is a cosine expansion where one can use a Fast Fourier Transform.

We will discuss two particular aspects of this numerical method: the preconditioning by an integral operator and the boundary constraints. The derivative operator is an ill-conditioned triangular matrix, whereas the integration operator is a banded matrix. Then

preconditioning the system by the appropriate order n integration operator results in a favorably conditioned system. The first n rows of the system become zero, and one can replace these with row vectors associated with the boundary constraints. See Coutsias *et al.*(1995) for further details.

6.1. *Time-dependent Solver*

To investigate the transient and steady state behavior of the system, we implement a time-dependent solver. The spatial component is discretized using the pseudospectral method and the temporal component, as is customary in the use of spectral methods to solve PDEs, using a finite difference method. This code is described below.

6.2. *General Discussion*

Consider the equation

$$Pr\frac{\partial u}{\partial t} = Lu + f(r,t) + N(u)$$

where $f(r,t)$ is a forcing term and $N(u)$ is a nonlinear term. This code computes Lu and $f(r,t)$ implicitly and $N(u)$ explicitly. Thus the Implicit-Explicit (IMEX) scheme Ascher *et al.*(1995) is given by

$$\frac{Pr}{\Delta t}\sum_{k=-r}^{1} a_k u^{n+k} = Lu^{n+1} + \sum_{k=-r}^{0} b_k N(u^{n+k}) \tag{6.1}$$

to get

$$a_1 u^{n+1} - \frac{\Delta t}{Pr}Lu^{n+1} = \sum_{k=-r}^{0}\left(-a_k u^{n+k} + \frac{\Delta t}{Pr}b_k N(u^{n+k})\right) + \frac{\Delta t}{Pr}f(r,t)^{n+1}$$

where u^n indicates the solution at time step n and the coefficients a_k and b_k are given in appendix C.

6.3. *The Helmholtz Operator*

Now implement the above procedure where L is a Helmholtz operator. In this code, there are two operators, one for temperature and one for velocity. In considering the equation governing the evolution of the temperature variables, $L = \nabla^2 - \sigma^2 I$ and equation (6.1) becomes

$$([1 + \frac{\sigma^2}{Pra_1}\Delta t]I - \frac{1}{Pra_1}\Delta t\nabla^2)u^{n+1} =$$
$$\frac{1}{a_1}\sum_{k=-r}^{0}\left(-a_k u^{n+k} + \frac{1}{Pr}\Delta t b_k N(u^{n+k})\right) + \frac{1}{Pra_1}\Delta t f(r,t)^{n+1}.$$

In the equation governing the evolution of the velocity variables the operator is the Laplacian, $L = \nabla^2$, and equation (6.1) becomes

$$\left(\frac{1}{Pr} - \frac{1}{Pra_1}\Delta t\nabla^2\right)w^{n+1} = \frac{1}{Pra_1}\sum_{k=-r}^{0}\left(-a_k w^{n+k}\right) + \frac{1}{a_1}\Delta t f(r,t)^{n+1}.$$

6.4. *Inverting the Helmholtz Operator*

In the solution of the system, one must invert the operator. Again, there are two different operators in this code, and each is inverted as follows.

In the equation governing the evolution of the temperature variables, let $\alpha = \frac{1}{Pra_1}\Delta t$ and $\beta = 1 + \frac{\sigma^2}{Pra_1}\Delta t$. Thus one must solve an equation of the form

$$(\beta I - \alpha\nabla^2)u = g$$

where g contains the nonlinear terms. In cylindrical coordinates one arrives at

$$(\beta I - \alpha\frac{1}{r}[\partial_r r\partial_r])u = g$$

$$(\beta R - \alpha[\partial_r^2 r - \partial_r])u = Rg$$

$$(\beta B_{[2]}^2 R + \alpha[B_{[2]} - R_{[2]}])u = B_{[2]}^2 Rg$$

where B represents the preconditioning matrix that is an integral operator, the subscript $_{[*]}$ denotes the number of top rows that are zero rows, and R represents the matrix that is multiplication by r. See appendix D for details.

In the equation governing the evolution of the velocity variable, let $\gamma = \frac{1}{Pr}$. Thus one must solve an equation of the form

$$(\gamma I - \alpha\nabla^2)u = g,$$

again, where g contains the nonlinear terms. In cylindrical coordinates one arrives at

$$(\gamma I - \alpha\frac{1}{r}[\partial_r r\partial_r])u = g$$

$$(\gamma R - \alpha[\partial_r^2 r - \partial_r])u = Rg$$

$$(\gamma B_{[2]}^2 R + \alpha[B_{[2]} - R_{[2]}])u = B_{[2]}^2 Rg.$$

6.5. *The Code*

To solve the system 2.12–2.14, the code performs the following steps.

- Initialize boundary values and boundary constraints
- Initialize variables
- Create and factor operators

while($t < tstop$)

- Evaluate nonlinear terms in point space
- Precondition ϕ and ψ variables and their right hand sides
- Time step and solve for ϕ, ψ
- Precondition right hand side for w
- Time step and solve for w

end while

Velocity profiles and time-series plots that result from this code are given in section 7.2.

Discussion of the use of implicit-explicit schemes is found in the paper by Ascher *et al*, Ascher *et al.*(1995).

The Newton code, discussed in the next section, provides verification of steady state results obtained via the time dependent code. In particular, for a given discretization, Gr and Pr, time steps of a size that will find the same solution as the Newton code are employed.

As an alternate means to find the steady state flow, we have developed a Newton code that directly finds a steady state flow. This code has the advantage over the time-dependent solver of quickly locating a steady state solution, and the matrices used in the Newton code are used in finding the eigenvalues of the system, making the task of

locating eigenvalues trivial. However, this code cannot be of use in analyzing transient phenomena or in analyzing time-dependent flows.

6.6. *General Discussion*

For the system 2.12—2.14, in the limiting case $\sigma = 0$, the problem is formulated so that a steady solution can be found.

$$Pr\phi_t = \nabla^2\phi + Gr\psi w$$

$$Pr\psi_t = \nabla^2\psi - Gr\phi w$$

$$w_t = \nabla^2 w + Pr\phi$$

Set the time derivatives to 0. One can write the resulting system as

$$\nabla^2(\mathbf{u}) + F(\mathbf{u}) = 0$$

where

$$\mathbf{u} = \begin{pmatrix} \phi \\ \psi \\ w \end{pmatrix}; F(\mathbf{u}) = \begin{pmatrix} Gr\psi w \\ -Gr\phi w \\ Pr\phi \end{pmatrix}.$$

At each iterate update the current solution $\mathbf{u}^n$ by $\delta\mathbf{u}$:

$$\nabla^2(\mathbf{u}^n + \delta\mathbf{u}) + F(\mathbf{u}^n + \delta\mathbf{u}) = 0.$$

Using Taylor's theorem gives

$$\nabla^2(\delta\mathbf{u}) + F_{\mathbf{u}}(\mathbf{u}^n)\delta\mathbf{u} = -(\nabla^2\mathbf{u}^n + F(\mathbf{u}^n)),$$

which leads to the system

$$\left(\begin{bmatrix} \nabla^2 & & \\ & \nabla^2 & \\ & & \nabla^2 \end{bmatrix} + \begin{bmatrix} 0 & Grw^n & Gr\psi^n \\ -Grw^n & 0 & -Gr\phi^n \\ PrI & 0 & 0 \end{bmatrix}\right)\begin{pmatrix} \delta\phi \\ \delta\psi \\ \delta w \end{pmatrix} =$$
$$-\left(\begin{bmatrix} \nabla^2 & & \\ & \nabla^2 & \\ & & \nabla^2 \end{bmatrix}\begin{pmatrix} \phi^n \\ \psi^n \\ w^n \end{pmatrix} + \begin{pmatrix} Gr\psi^n w^n \\ -Gr\phi^n w^n \\ Pr\phi^n \end{pmatrix}\right).$$

For ease of notation, define the right hand side to be $\mathbf{g}$. At each iterate $\mathbf{u}^n$ is known and the task is to solve for δu.

Now, in this case, use the vector $\mathbf{u}$ in Chebyshev modespace, and so in the usual way (see appendix D) write the spectral operators to get the system:

$$\left(\begin{pmatrix} R-B & & \\ & R-B & \\ & & R-B \end{pmatrix} + \right.$$
$$\left.\begin{pmatrix} B^2R & & \\ & B^2R & \\ & & B^2R \end{pmatrix}\begin{pmatrix} 0 & Grw^n* & Gr\psi^n* \\ -Grw^n* & 0 & -Gr\phi^n* \\ PrI* & 0 & 0 \end{pmatrix}\right)\begin{pmatrix} \delta\phi \\ \delta\psi \\ \delta w \end{pmatrix} =$$
$$\begin{pmatrix} B^2R & & \\ & B^2R & \\ & & B^2R \end{pmatrix}\mathbf{g},$$

where $*$ signifies convolution. The Newton code forms these matrices and solves this system. However, a further simplification must be made in order to solve the system.

Because the function $\mathbf{u}$ is an even function, the symmetry of the system is important in the method of solution. The operator has nonzero entries in (even row, odd column) positions (counting from 0 so that matrix entries correspond to the Chebyshev polynomials). The right hand side has nonzero entries in odd row positions. The solution must be an even function, so it has entries in the even row positions. If one were to attempt to solve the system with the zeros that exist due to symmetry, the operator would be singular and one would not be able to do it. Instead, pack the system, keeping only the odd row, even column entries. One is then able to solve this system, which is half as large as the original. We use the Lapack routines dgeco and dgesl to factor and solve the system, respectively.

6.7. *The Code*

The code performs the following steps.

- Read in parameters, vector $\mathbf{u}$
- Create B, R, I, B^2R
- Make Laplacian
- Make preconditioner
- Enter the loop while error $>$ tol
  - Create convolution
  - Precondition convolution
  - Create , precondition packed operator
  - Implement boundary constraint on operator
  - Create, precondition rhs
  - Implement boundary condition on rhs
  - Pack rhs
  - Factor
  - Solve
  - Update $\mathbf{u}$, error

6.8. *The Eigenvalue Problem*

Again, consider the system 2.12—2.14,

$$Pr\phi_t = \nabla^2\phi + Gr\psi w$$

$$Pr\psi_t = \nabla^2\psi - Gr\phi w$$

$$w_t = \nabla^2 w + Pr\phi$$

Assuming a separable solution, the solution is

$$\mathbf{u} = \mathbf{u}(r)e^{i\lambda t}.$$

Expanding the solution in powers of ϵ gives

$$\mathbf{u} = \mathbf{u}_0 + \epsilon\mathbf{u}_1 + O(\epsilon^2).$$

Then the order ϵ system is

$$\left(\begin{bmatrix} \nabla^2 & & \\ & \nabla^2 & \\ & & \nabla^2 \end{bmatrix} + \begin{bmatrix} 0 & Grw_1* & Gr\psi_1* \\ -Grw_1* & 0 & -Gr\phi_1* \\ PrI* & 0 & 0 \end{bmatrix}\right)\begin{pmatrix} \phi_1 \\ \psi_1 \\ w_1 \end{pmatrix}$$

$$= \lambda\left(\begin{bmatrix} Pr & & \\ & Pr & \\ & & I \end{bmatrix}\begin{pmatrix} \phi_1 \\ \psi_1 \\ w_1 \end{pmatrix}\right).$$

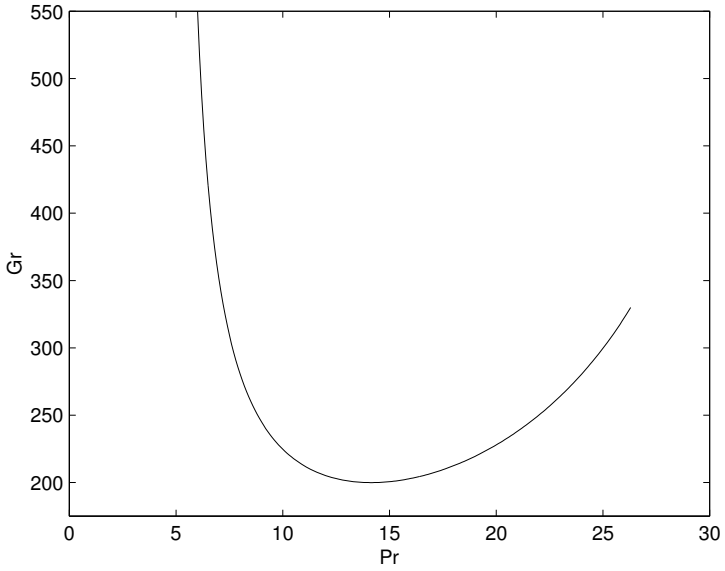

FIGURE 4. The location of the Hopf bifurcation in the PDE model

This is the generalized eigenvalue problem $A\mathbf{x} = \lambda B\mathbf{x}$. Note that the left hand side matrices are identical to those formed for the Newton iteration; thus one only need create the mass matrix B of time-dependent coefficients in order to solve the eigenvalue problem. We use the Lapack routine dggev to compute the generalized eigenvalues and the left and right eigenvectors.

Results from the implementation of this eigenvalue code are found in section 7.4.

Using this code one can map the locus of the onset of the Hopf bifurcations for a given Prandtl number. Graphs of this bifurcation diagram are shown in 4.

7. Conclusions

7.1. *Bifurcations*

For the initial bifurcation (section B), the critical Grashof number is found to be $Gr_c = \frac{\gamma_{01}^4}{Pr}$; that is, one can view the critical parameter as $Ra_c = \gamma_{01}^4$. This is in qualitative agreement with models that use the Lorenz equations, where the initial bifurcation point is at the constant $R = 1$. Using equation A, the Lorenz equations predict that the system will become convective at $Ra = 64$; in fact, from our analysis, it becomes unstable at $Ra \approx 33$, so the Lorenz equations overpredict the region where the trivial solution is stable.

The Lorenz equations predict that the Hopf bifurcation exists at $Gr = \frac{64(Pr+4)}{Pr-2}$; for $Pr = 7$, for example, this is $Gr = 140.8$, where our analysis shows it is unstable at $Gr \approx 350$; here, the Lorenz equations underpredict the region where the convective solution is stable. Compare the curves of the predicted Hopf bifurcation, by the Lorenz equation in figure 5 and calculated with the PDE model in figure 4. Both exhibit a vertical asymptote as a lower bound, but the shape of the curve differs significantly as Pr grows. Figure 4 shows the location of the Hopf bifurcation as a function of Prandtl number. Notice that there is a vertical asymptote to the right of $Pr = 5$. That is, there is a region of Pr values for which there is no Hopf bifurcation. This result is in qualitative

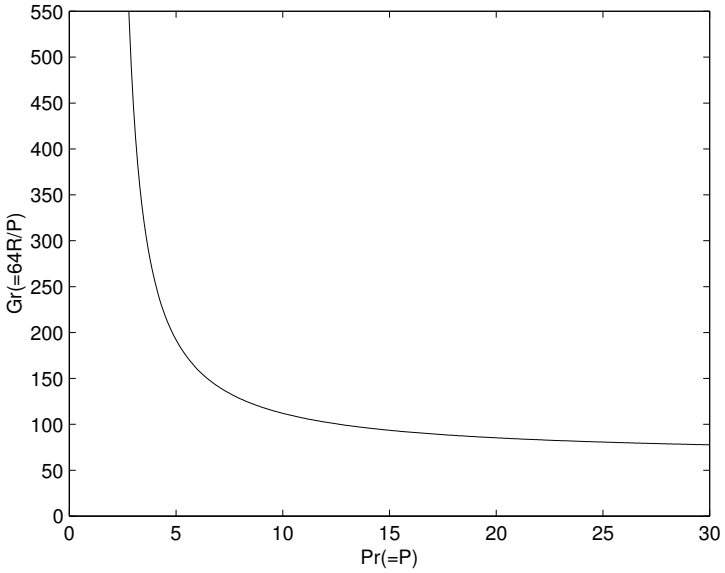

FIGURE 5. The location of the Hopf bifurcation in the Lorenz equations, in terms of the dimensionless parameters Pr and Gr

agreement with the Lorenz equations. However, there appears to be no upper limit where there ceases to exist a Hopf bifurcation.

Now, there does seem to be significant difference between the Lorenz model and our reduced PDE model in predicting whether the Hopf bifurcation is sub- or supercritical. As discussed in section 4.2, our PDE model predicts that the Hopf bifurcation is subcritical for Prandtl numbers less than ≈ 19 and supercritical for Prandtl numbers greater than that. The Lorenz equations, on the other hand, predict that the Hopf bifurcation is subcritical for this entire range of values. Noting the significant difference in the shape of the curves 4 and 5, it seems clear that the Lorenz model is not as accurate a model for flow in a thermosyphon for large Prandtl numbers.

7.2. *Velocity and Temperature Profiles*

Running the time integration code allows us to view the transient nature of the system, as well as observe the converged profiles at the final steady state.

First we will comment on the profiles for Pr=1. There is no Hopf bifurcation at this Prandtl number. The profiles for all variables maintain a parabolic-like shape for low Grashof numbers, although for a large Grashof number, $Gr = 100$, (figure 7) the profile for ϕ, the sine coefficient of temperature, has flattened. At a much higher Grashof number, $Gr = 350$ (figure 8) it has formed a "dip," where the maximum value is no longer at the center. This grows more extreme as Grashof increases. When $Gr = 550$ (figure 9) the dip has become so severe that there it is almost zero at the center. Notice, then, that in the corresponding velocity profiles, that this action serves to slow the flow down, and that it remains a parabolic-like velocity profile where the maximum velocity is quite small.

Contrast this to the scenario for a higher Prandtl number, $Pr = 7$, where the Hopf bifurcation does occur. Near the Hopf bifurcation point, $Gr = 350$ (figure 10) the velocity profile is not a parabolic profile; rather it has developed a "dip." Notice that it is the ϕ component of temperature that drives this change. These profiles clearly show how the

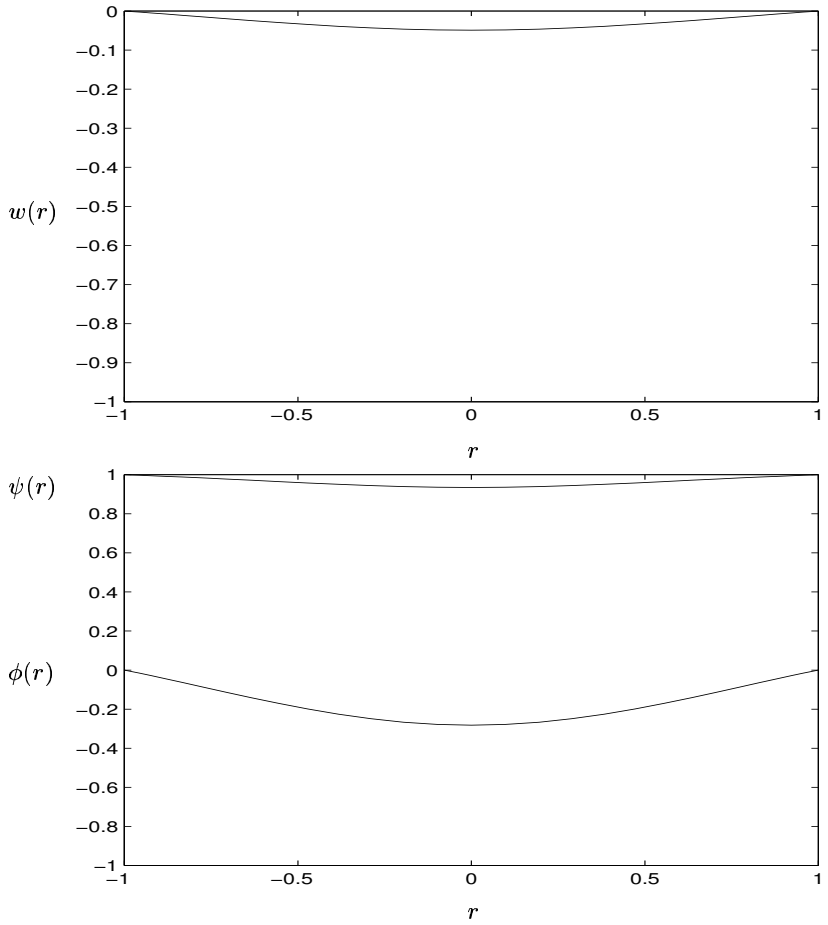

FIGURE 6. Velocity and temperature profiles at Prandtl=1, Grashof=35

Lorenz model will not accurately capture the dynamics of the flow in the regions where the profiles are not parabolic.

Figure 11 illustrates the similarity in the velocity profiles for various Prandtl numbers.

7.3. *Bifurcation Diagram*

In figure 13 the bifurcation diagram is shown for $Pr = 7$. Notice that the thermosyphon runs most efficiently for Grashof number around 10. For values of Grashof greater than 10, the velocity slows. From the temperature profiles shown in figures 6– 9, this loss of efficiency is seen as the ϕ component develops a quartic profile.

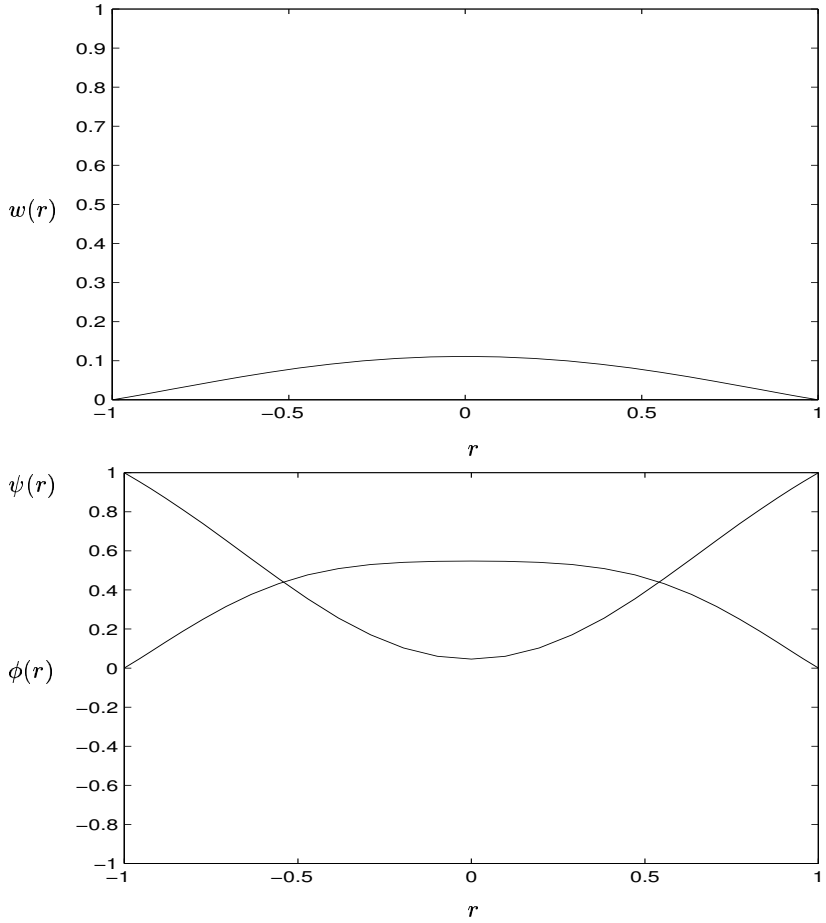

FIGURE 7. Velocity and temperature profiles at Prandtl=1, Grashof=100

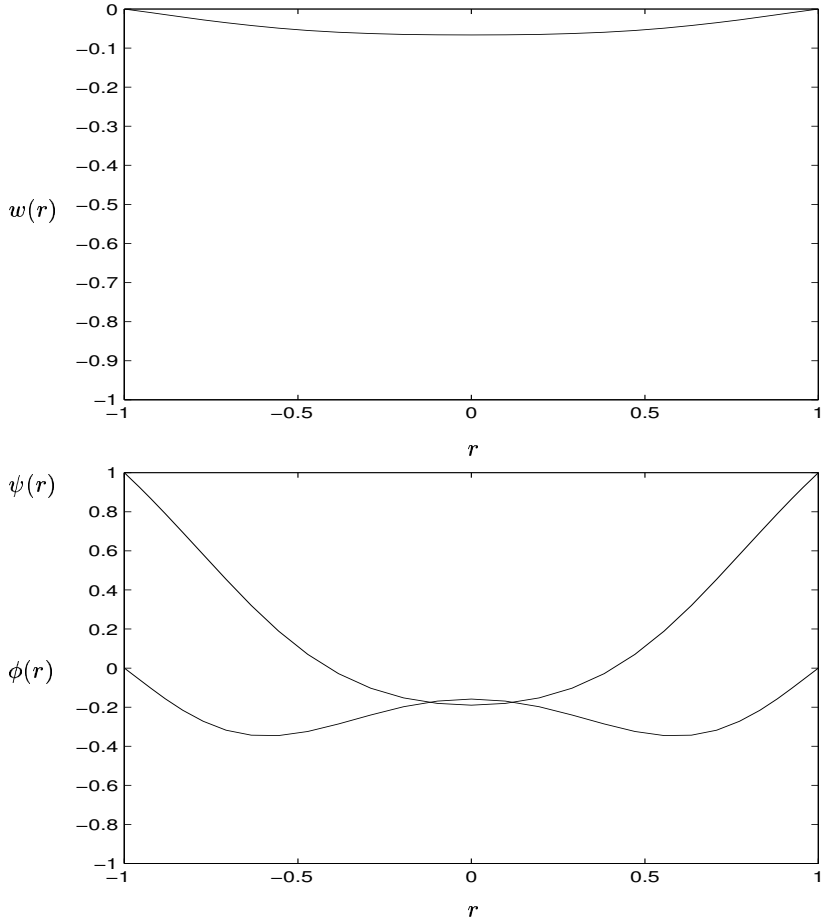

FIGURE 8. Velocity and temperature profiles at Prandtl=1, Grashof=350

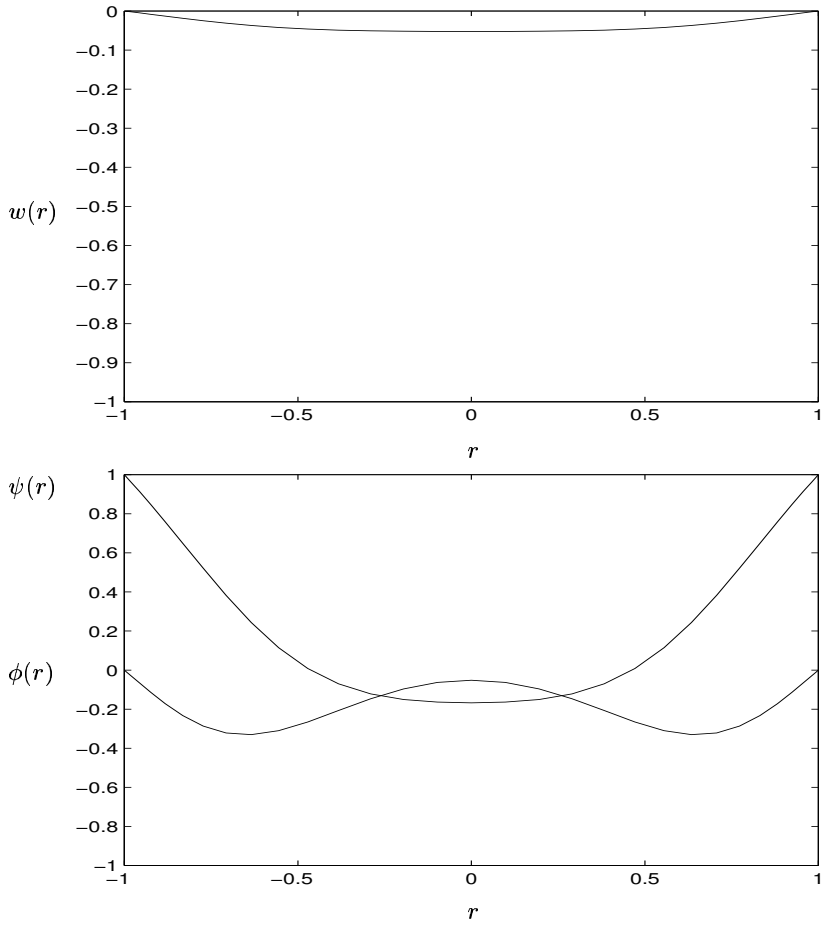

FIGURE 9. Velocity and temperature profiles at Prandtl=1, Grashof=550

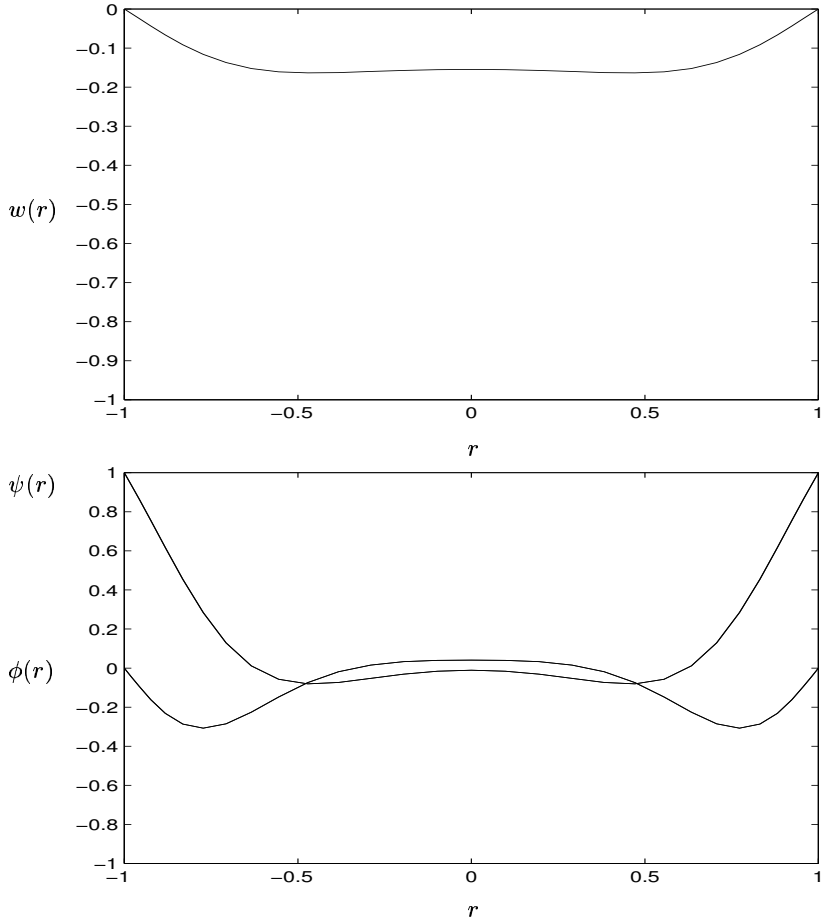

FIGURE 10. Velocity and temperature profiles at Prandtl=7, Grashof=350

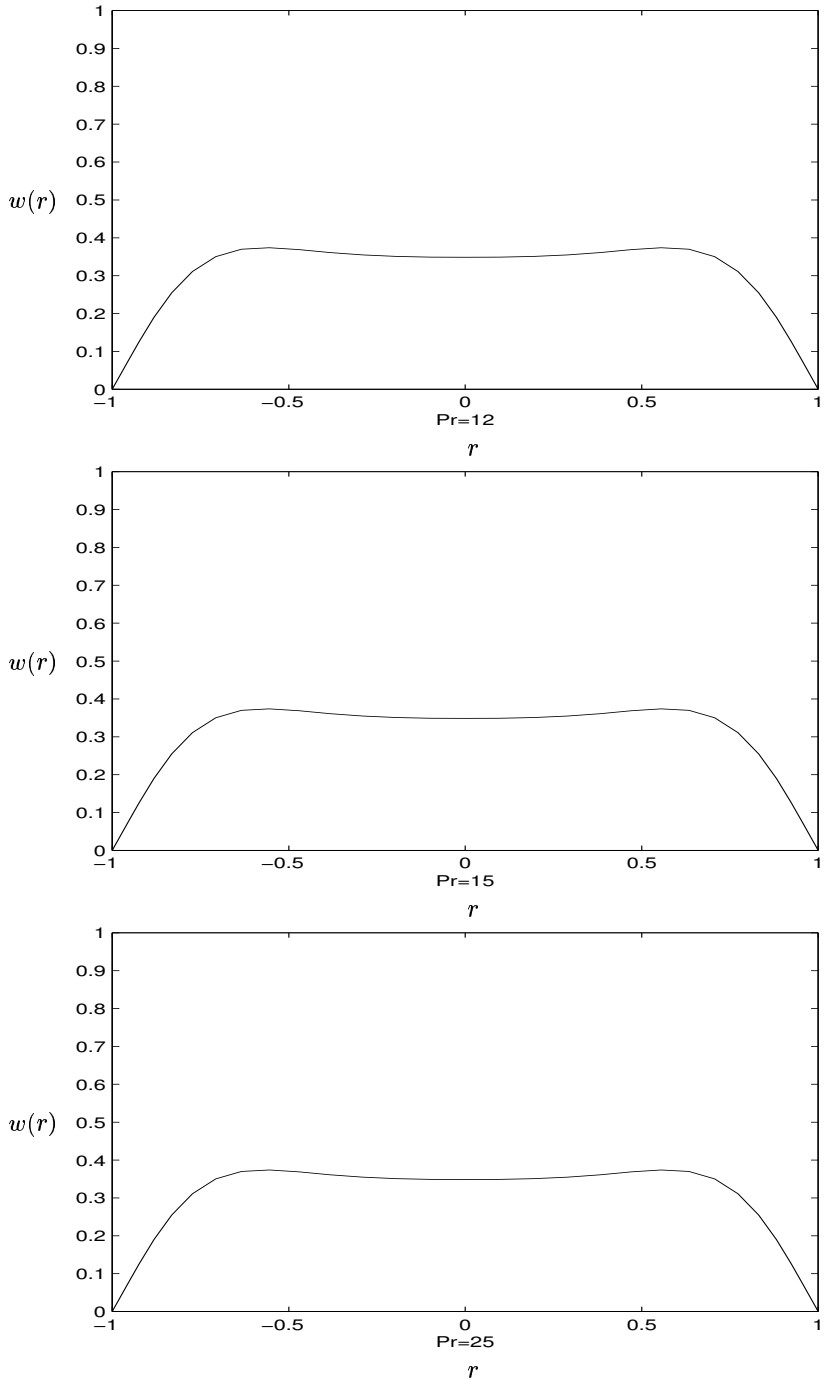

FIGURE 11. Velocity profiles at the Hopf bifurcation point for various Prandtl numbers.

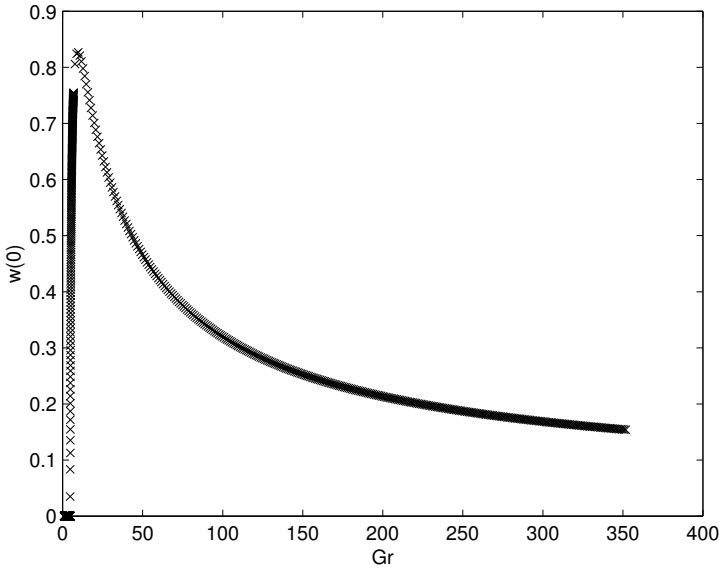

FIGURE 12. The bifurcation diagram at $Pr = 7$

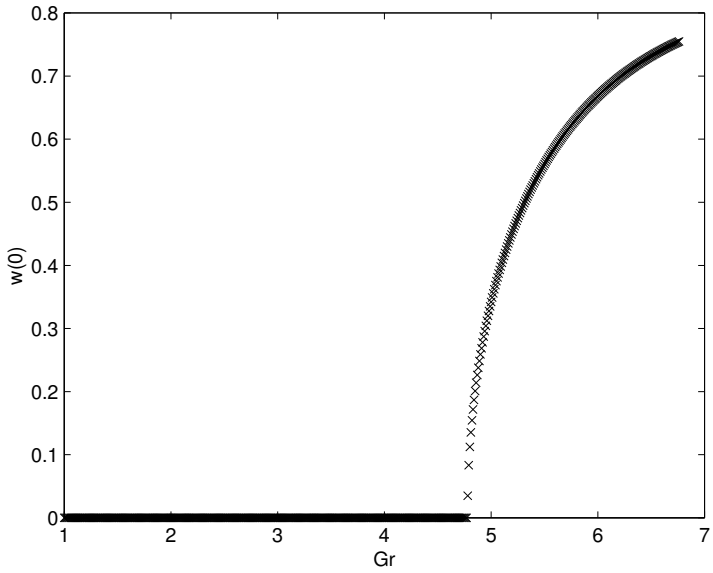

FIGURE 13. An enlargement of the pitchfork bifurcation at $Pr = 7$.

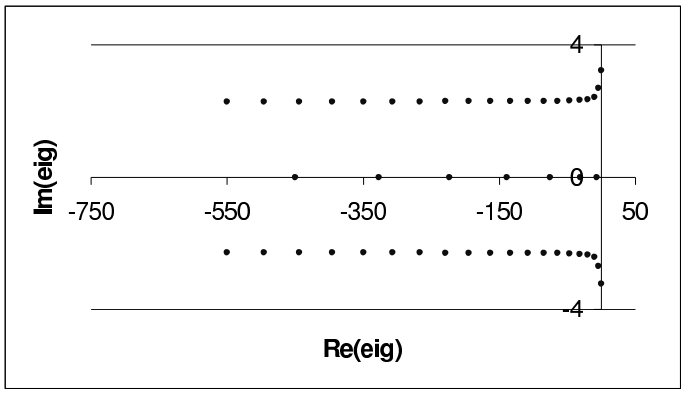

FIGURE 14. Eigenvalues at Pr=7, Gr=50.

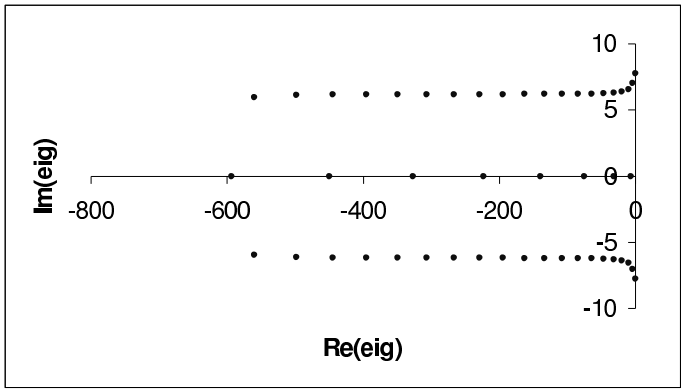

FIGURE 15. Eigenvalues at Pr=7, Gr=300.

7.4. *Eigenvalue Results*

Table 3 illustrates the convergence of the eigenvalues with mesh refinement. Notice that for a variety of Gr numbers, 32 modes is sufficient to find the eigenvalue to 8 significant figures. This is not the case for the eigenvectors, however. In some cases, there are steep slopes in the eigenvector profiles, requiring a higher resolution.

Plots 14 – 15 demonstrate the discrete spectrum of the discretized operator.

$Gr = 4$			
N	λ_1	λ_2	λ_3
16	-0.11986932	-0.82616942	-4.20077833
32	-0.11986928	-0.82616942	-4.20077531
64	-0.11986928	-0.82616942	-4.20077531
128	-0.11986928	-0.82616942	-4.20077531
$Gr = 5$			
16	$3.3436286822 \times 10^{-2}$	-0.82616942	-4.16298621
32	$3.3436286827 \times 10^{-2}$	-0.82616942	-4.16298317
64	$3.3436286827 \times 10^{-2}$	-0.82616942	-4.16298317
128	$3.3436286827 \times 10^{-2}$	-0.82616942	-4.16298317
$Gr = 10$			
16	$-0.38966583 \pm 1.06623072i$	$-4.22920743 \pm 0.83528015i$	-6.71435768
32	$-0.38967750 \pm 1.06625057i$	$-4.22924245 \pm 0.83529406i$	-6.71433609
64	$-0.38967750 \pm 1.06625057i$	$-4.22924245 \pm 0.83529406i$	-6.71433609
128	$-0.38967750 \pm 1.06625057i$	$-4.22924245 \pm 0.83529406i$	-6.71433609
$Gr = 50$			
16	$-0.29153807 \pm 3.22110087i$	$-4.08359747 \pm 2.68818657i$	-7.10593143
32	$-0.29158500 \pm 3.22112920i$	$-4.08324280 \pm 2.68805007i$	-7.10590921
64	$-0.29158500 \pm 3.22112920i$	$-4.08324280 \pm 2.68805007i$	-7.10590921
128	$-0.29158500 \pm 3.22112921i$	$-4.08324280 \pm 2.68805007i$	-7.10590921
$Gr = 300$			
16	$-2.86 \times 10^{-2} \pm 7.76286427i$	$-3.98176664 \pm 7.04824907i$	-7.06274178
32	$-2.74 \times 10^{-2} \pm 7.76272788i$	$-3.98493589 \pm 7.05070856i$	-7.06544438
64	$-2.74 \times 10^{-2} \pm 7.76272788i$	$-3.98493592 \pm 7.05070859i$	-7.06544440
128	$-2.74 \times 10^{-2} \pm 7.76272788i$	$-3.98493592 \pm 7.05070859i$	-7.06544440
$Gr = 350$			
16	$-2.30 \times 10^{-3} \pm 8.34640116i$	$-3.95978468 \pm 7.60465151i$	-7.03438673
32	$-8.37 \times 10^{-4} \pm 8.34580017i$	$-3.96462820 \pm 7.60592416i$	-7.03555062
64	$-8.37 \times 10^{-4} \pm 8.34580016i$	$-3.96462826 \pm 7.60592417i$	-7.03555065
128	$-8.37 \times 10^{-4} \pm 8.34580016i$	$-3.96462826 \pm 7.60592417i$	-7.03555065

TABLE 3. The first three eigenvalues of flow in a thermosyphon with $Pr = 7.0$ N=number of modes.

7.5. *Three-Dimensional Calculations With MPSalsa*

We will discuss the numerical methods used by MPSalsa to locate steady state solutions of Equations (2.1)–(2.3), the formulation of the eigenvalue problem and the Cayley transform method, and the numerical solution of the eigenvalue problem.

7.6. *Spatial Discretization and the Non-linear Solve*

A full description of the numerical methods in MPSalsa used to locate steady state solutions of Equations (2.1)–(2.3) is available in Shadid(1999) and the references listed therein. A brief overview is presented in this section.

A mesh of quadrilaterals for 2D problems and hexahedra for 3D problems is generated to cover the domain. Although the code allows for general unstructured meshes, this problem uses structured meshes. For parallel runs, the mesh is partitioned using the Chaco code Hendrickson & Leland(1995) in a way that will distribute work evenly while minimizing communication costs between processors. A Galerkin/least-squares finite element method Hughes *et al.*(1989) (GLS-FEM) is used to discretize the time-invariant versions of the governing partial differential equations (2.1)–(2.3) into a set of nonlinear algebraic equations. This formulation includes a pressure stabilization term so that the velocity components, temperature and pressure fields can all be represented with equal order nodal basis functions. GLS-FEM is a consistent stabilized scheme because when the exact solution is inserted, the Boussinesq equations are satisfied exactly. The code uses bilinear and trilinear nodal elements for two and three dimensional problems, respectively.

Discretization of (2.1)–(2.3) results in the matrix equation

$$\begin{pmatrix} \mathbf{M} & \mathbf{0} \\ \mathbf{N} & \mathbf{0} \end{pmatrix} \begin{bmatrix} \dot{\mathbf{u}} \\ \dot{\mathbf{p}} \end{bmatrix} + \begin{pmatrix} \mathbf{K}_{u,T} + \mathbf{C}(\mathbf{u}) & -\mathbf{D} \\ \mathbf{D}^T + \mathbf{G} & \mathbf{K}_p \end{pmatrix} \begin{bmatrix} \mathbf{u} \\ \mathbf{p} \end{bmatrix} - \begin{bmatrix} \mathbf{g} \\ \mathbf{h} \end{bmatrix} = \begin{bmatrix} \mathbf{0} \\ \mathbf{0} \end{bmatrix} \tag{7.1}$$

where $\mathbf{u}$ is the vector of fluid velocity components and temperature unknowns, $\mathbf{p}$ is the pressure, $\mathbf{M}$ is the symmetric positive definite matrix of the overlaps of the finite element basis functions, $\mathbf{K}_{u,T}$ is the stiffness matrix associated with velocity and temperature, $\mathbf{C}(\mathbf{u})$ is the nonlinear convection, $\mathbf{D}$ is the discrete (weak) gradient, $\mathbf{D}^T$ is the discrete (weak) divergence operator and $\mathbf{K}_p$ is the stiffness matrix for the pressure. $\mathbf{G}, \mathbf{K}_p, \mathbf{N}$ are stabilization terms arising from the GLS-FEM. The vectors $\mathbf{g}$ and $\mathbf{h}$ denote terms due to boundary conditions and the Boussinesq approximation.

The resulting nonlinear algebraic equations arising from setting the time derivative terms to zero are solved using a fully coupled Newton-Raphson method Shadid *et al.*(1997). An analytic Jacobian matrix for the entire system is calculated and stored in a sparse matrix storage format. At each Newton-Raphson iteration, the linear system is solved using the Aztec package Tuminaro *et al.*(1999) of parallel preconditioned Krylov iterative solvers. The accuracy of the steady state solve is set by the following stopping criterion,

$$\left(\frac{1}{N} \sum_{i=1}^{N} \left(\frac{|\delta_i|}{\epsilon_R |x_i| + \epsilon_A} \right)^2 \right)^{\frac{1}{2}} < 1.0,$$

where ϵ_R and ϵ_A are the relative and absolute tolerances desired, δ_i is the update for the unknown x_i and N is the total number of unknowns. We use relative and absolute tolerances of 10^{-5} and 10^{-8}, respectively, for this study. In Aztec the code exclusively uses an unrestarted GMRES iteration with a non-overlapping Schwarz preconditioner where an ILU preconditioner is used on each sub-domain (each processor contains one sub-domain). These methods enable rapid convergence to both stable and unstable steady state solutions. The scalability of these methods to large system sizes and numbers of

processors is demonstrated by the solution of a 16 million unknown model on 2048 processors Burroughs *et al.*(2001).

7.7. *The Discretized Eigenvalue Problem and Cayley Transforms*

The GLS-FEM results in a spatial discretization of the Navier-Stokes equations with the Boussinesq approximation. This leads to a finite dimensional system of differential algebraic equations of the form

$$\mathbf{B}\dot{\mathbf{x}} = \mathbf{F}(\mathbf{x}), \qquad \mathbf{x}(0) = \mathbf{x}_0, \tag{7.2}$$

where the matrix $\mathbf{B}$ is singular (due to the divergence free constraint) and $\mathbf{x}$ is a vector containing the nodal values of the velocities, temperature and pressure at the nodes of the finite element mesh. Because of the stabilization terms in the GLS discretization, $\mathbf{B}$, the matrix associated with the time derivative term in (7.1), is a non-symmetric matrix.

Solve the generalized eigenvalue problem

$$\lambda\mathbf{B}\mathbf{z} = \mathbf{J}(\mathbf{x}_s)\mathbf{z} \equiv \mathbf{J}\mathbf{z}. \tag{7.3}$$

that arises from the linearization of (7.2) about the steady state. The matrix $\mathbf{J}(\mathbf{x}_s)$ is the Jacobian of $\mathbf{F}(\cdot)$ linearized about $\mathbf{x}_s$. Assume that the eigenvalues are ordered with respect to decreasing real part; $\text{real}(\lambda_{i+1}) \leq \text{real}(\lambda_i)$. If all the eigenvalues of (7.3) have negative real parts, the steady state is stable.

Use a Cayley transform to find the eigenvalues γ_i of the system

$$(\mathbf{J} - \sigma\mathbf{B})^{-1}(\mathbf{J} - \mu\mathbf{B})\mathbf{z} = \gamma\mathbf{z}$$

that are related to the eigenvalues λ_k of (7.3) via

$$\gamma_i = \frac{\lambda_k - \mu}{\lambda_k - \sigma} \quad i = 1, \ldots, n; k = 1, \ldots, n$$

Choose $\sigma > 0$ and $\mu = -\sigma$; we choose the value of σ so that it is of similar magnitude to the imaginary part of the eigenvalue of interest, and so that $\sigma > Re(\lambda_1)$. This transformation has the property of mapping a λ in the right half of the complex plane (i.e. an unstable mode) to a γ outside the unit circle, and those on the left half plane (i.e. a stable mode) to a γ inside the unit circle. That is,

$$\text{real}(\lambda) > 0 \Longrightarrow \|\gamma\| > 1.0, \; \textit{and} \; \text{real}(\lambda) < 0 \Longrightarrow \|\gamma\| < 1.0.$$

Since Arnoldi's method will converge more rapidly to those eigenvalues with larger magnitudes, this is a very desirable property for calculating eigenvalues for use in linear stability analysis.

Further details are available in the papers Lehoucq & Salinger(2001), Burroughs *et al.*(submitted 2002).

7.8. *Three-dimensional Results*

We will compare results for the most unstable eigenvalue from the spectral eigenvalue code presented in chapter 6 with the results computed using the finite element code. In MPSalsa set $g = \beta = \kappa = \nu = 1$ and $f(\theta) = \cos(\theta)$. The mesh has $\frac{N}{4}$ by $\frac{N}{4}$ mesh divisions around a cross-section and $N + \frac{N}{20}$ mesh divisions about the circumference of the loop. Results for various values of N are reported in tables 4, for $Pr = 1$ and 5 for $Pr = 7$. For the finest mesh, there are 185,220 unknowns, solved on 64 processors of the Sandia-Intel TFlop machine (ASCI Red) with 333 MHz Pentium processors. The code converges to the steady state easily using a zero initial guess. The number of GMRES solves for each eigensolver iteration is approximately 240. The time to compute eigenvalues on the finest

N	$Ra_{therm} = 30$	$Ra_{therm} = 32.5$	$Ra_{therm} = 35$	$Ra_{therm} = 37.5$
20	-0.758	-0.533	-0.316	-0.108
40	-0.389	-0.163	0.054	0.264
80	-0.303	-0.078	0.139	0.348
asymptotic	-0.306	-0.082	0.133	0.341

TABLE 4. The first eigenvalue of flow in a thermosyphon with $R_T = 1$, $R_H = 10$, $Pr = 1.0$, $\frac{N^2}{16} \times (N + \frac{N}{20})$ uniform mesh

N	$Ra_{therm} = 30$	$Ra_{therm} = 32.5$	$Ra_{therm} = 35$	$Ra_{therm} = 37.5$
20	-0.176	-0.123	-0.0705	-0.0189
40	-0.0967	-0.0370	0.0171	0.0704
80	-0.0713	-0.0158	0.0387	0.0923
asymptotic	-0.0753	-0.0205	0.0345	0.0865

TABLE 5. The first eigenvalue of the trivial branch for flow in a thermosyphon with $R_T = 1$, $R_H = 10$, $Pr = 7.0$, $\frac{N^2}{16} \times (N + \frac{N}{20})$ uniform mesh

mesh is 2671 seconds for Ra=30. Once N is large enough, there is good agreement between the asymptotic and numerical results. Notice that the critical value is independent of Prandtl number, and this is confirmed by the three-dimensional calculations.

7.9. *Summary*

An examination of flow in a thermosyphon has been conducted using a new PDE model of flow in a thermosyphon. In the case of a circular loop, the first Fourier modes exactly decouple from all other Fourier modes, leaving a system of three coupled nonlinear PDEs that completely describe the flow in the thermosyphon. This is in contrast to all existing models, which use truncations, adjustable parameters, and other simplifications that are avoided in this formulation.

The use of this model has allowed the identification of stable periodic flows that are not found using Lorenz-type ODE models. In particular, this model has identified periodic solutions for flows of Prandtl number greater than 19.

The trivial solution was found to be globally stable for all Prandtl numbers for $Ra < \gamma^4$, where γ is the first zero of the J_0 Bessel function. This global stability limit coincides with the location of the first bifurcation, indicating the onset of convection in the thermosyphon.

Appendix A. Reduction to the Lorenz model

The Lorenz equations Lorenz(1963) are a set of ordinary differential equations that, for certain parameter values, provide a simple model of flow in a thermosyphon. Most reported investigations of the thermosyphon problem use a reduction to the Lorenz equa-

tions. This type of model exhibits the flow pattern of convection leading to oscillation and chaos. We will compare the simplified PDE model (2.12—2.14) to the Lorenz model by imposing a parabolic profile on each of the variables and substituting this into the equations. For simplicity, we will neglect the curvature term on the right hand side of the ϕ and ψ equations.

It is the assumption of a parabolic profile that leads to the most significant limitations of the Lorenz model. In the flow profiles shown in section 7.2, one can see that for high values of the Grashof number the profiles deviate dramatically from a parabolic profile. The PDE model proves to be a better model for capturing the nature of the flow in this region.

To derive the Lorenz model, substitute into (2.12), (2.13), and (2.14)

$$w(r,t) = \hat{w}(t)(r^2 - 1)$$

$$\phi(r,t) = \hat{\phi}(t)(r^2 - 1)$$

$$\psi(r,t) = \psi_0 + \hat{\psi}(t)(r^2 - 1),$$

and integrate over a circle of radius 1 to get:

$$\frac{d\hat{w}}{dt} = -8\hat{w} + Pr\hat{\phi}$$

$$\frac{d\hat{\phi}}{dt} = -\frac{8}{Pr}\hat{\phi} - \frac{2Gr}{3Pr}\hat{\psi}\hat{w} + \frac{Gr\psi_0\hat{w}}{Pr}$$

$$\frac{d\hat{\psi}}{dt} = -\frac{8}{Pr}\hat{\psi} + \frac{2Gr}{3Pr}\hat{\phi}\hat{w}.$$

Now to correlate these equations to the Lorenz system, introduce

$$\hat{w} = \frac{3\psi_0 P}{16R}X$$

$$\hat{\phi} = \frac{3\psi_0}{2R}Y$$

$$\hat{\psi} = \frac{3\psi_0}{2R}Z$$

$$t = \frac{P}{8}T$$

$$Pr = P$$

$$Gr = \frac{64R}{\psi_0 P}$$

to arrive at the set of equations

$$\frac{dX}{dT} = -PX + PY$$

$$\frac{dY}{dT} = -Y + RX - XZ$$

$$\frac{dZ}{dT} = -Z + XY.$$

which correspond to the Lorenz system (see Tritton(1988)).

Appendix B. Pitchfork Analysis

B.1. *The Steady State Problem*

Considering zero order terms gives

$$\nabla^2 \begin{pmatrix} \phi_0 \\ \psi_0 \\ w_0 \end{pmatrix} + Gr_p \begin{pmatrix} 0 & 1 & 0 \\ -1 & 0 & 0 \\ 0 & 0 & 0 \end{pmatrix} \begin{pmatrix} \phi_0 \\ \psi_0 \\ w_0 \end{pmatrix} w_0 + \begin{pmatrix} 0 & 0 & 0 \\ 0 & 0 & 0 \\ Pr & 0 & 0 \end{pmatrix} \begin{pmatrix} \phi_0 \\ \psi_0 \\ w_0 \end{pmatrix} = 0$$

along with boundary conditions

$$\begin{pmatrix} \phi_0 \\ \psi_0 \\ w_0 \end{pmatrix} = \begin{pmatrix} 0 \\ 1 \\ 0 \end{pmatrix}.$$

The solution to this boundary value problem is easily found to be

B.2. *The Linear Problem*

At order ϵ one has the system

$$\nabla^2 \begin{pmatrix} \phi_1 \\ \psi_1 \\ w_1 \end{pmatrix} + \begin{pmatrix} 0 & 0 & Gr_p \\ 0 & 0 & 0 \\ Pr & 0 & 0 \end{pmatrix} \begin{pmatrix} \phi_1 \\ \psi_1 \\ w_1 \end{pmatrix} = 0 \tag{B 1}$$

along with null boundary conditions on the perturbation variables. The equation for ψ_1 decouples to give

$$\nabla^2 \psi_1 = 0,$$

which has solution

$$\psi_1 = 0.$$

The variables ϕ_1 and w_1 are described by the system

$$\nabla^2 \begin{pmatrix} \phi_1 \\ w_1 \end{pmatrix} = \begin{pmatrix} 0 & -Gr_p \\ -Pr & 0 \end{pmatrix} \begin{pmatrix} \phi_1 \\ w_1 \end{pmatrix}.$$

Using Bessel functions

$$\begin{pmatrix} \phi_{1,n} \\ w_{1,n} \end{pmatrix} = \begin{pmatrix} c_1 \\ c_2 \end{pmatrix} J_n(\gamma_{nm} r)$$

where

$$J_n(\gamma_{nm}) = 0$$

leads to the eigenvalue problem

$$-\gamma_{nm}^2 \begin{pmatrix} c_1 \\ c_2 \end{pmatrix} = \begin{pmatrix} 0 & -Gr_p \\ -Pr & 0 \end{pmatrix} \begin{pmatrix} c_1 \\ c_2 \end{pmatrix}.$$

Satisfying the condition

$$\begin{vmatrix} \gamma_{mn}^2 & -Gr_p \\ -Pr & \gamma_{mn}^2 \end{vmatrix} = 0$$

gives the critical parameter value for the pitchfork bifurcation,

$$Gr_p = \frac{\gamma_{mn}^4}{Pr}.$$

Gr_p is a minimum at γ_{01}, the first zero of the zero-order Bessel function. Note that this result correlates to the pitchfork bifurcation one finds in the Lorenz equations, where

the pitchfork bifurcation is a function of the Rayleigh number. Because $Gr = \frac{Ra}{Pr}$, this result can be written

$$Ra_p = \gamma_{01}^4.$$

The eigenvector is given by

$$\begin{pmatrix} c_1 \\ c_2 \end{pmatrix} = \begin{pmatrix} \gamma_{01}^2 \\ Pr \end{pmatrix}.$$

Appendix C. Hopf analysis

C.1. *Steady State Problem*

Considering the zero order terms gives

$$L_0 \mathbf{u}_0 = Gr_h u_{3,0} M \mathbf{u}_0$$

Solve the system to get the solution

$$\mathbf{u}_0 = \begin{pmatrix} u_{10} \\ u_{20} \\ u_{30} \end{pmatrix}.$$

This equation is solved numerically using the time-dependent solver and Newton algorithm described in section 6.

C.2. *Linear Problem*

At order ϵ one has the system

$$(L_0 - Gr_h J_0)\mathbf{u}_1 = -L_1 \mathbf{u}_0.$$

Note that $\mathbf{u}_0$ is a steady solution, so $L_1 \mathbf{u}_0 = 0$. Compute $\mathbf{u}_1$ by solving the resulting eigenvalue problem to get

$$\mathbf{u}_1 = a_1 \mathbf{A}(r) e^{is} + \bar{a}_1 \bar{\mathbf{A}}(r) e^{-is}$$

and ω_0. This eigenvalue problem is solved numerically using the eigenvalue code discussed in section 6.8.

C.3. *Bifurcation Analysis*

Continue with the analysis, now including higher order terms. Making the substitutions $s = \omega t$ and $\tau = \epsilon^2 s$, write the system as follows:

$$(\omega D \partial_s + \epsilon^2 D \partial_\tau - I\nabla^2 - A)\mathbf{u} = GrF(\mathbf{u}).$$

Expand the solution

$$\mathbf{u} = \mathbf{u}_0(r) + \epsilon \mathbf{u}_1(s, \tau, r) + \epsilon^2 \mathbf{u}_2(s, \tau, r) + \epsilon^3 \mathbf{u}_3(s, \tau, r) + O(\epsilon^4).$$

Expand the Grashof number as

$$Gr = Gr_h + j\epsilon^2,$$

where $j = \pm 1$, with $j = +1$ corresponding to $Gr > Gr_h$ and $j = -1$ corresponding to $Gr < Gr_h$. Expand the frequency as

$$\omega = \omega_0 + \epsilon \omega_1 + \epsilon^2 \omega_2.$$

This leads to the system

$$\left((\omega_0 D\partial_s - I\nabla^2 - A) + \epsilon\omega_1 D\partial_s + \epsilon^2(\omega_2 D\partial_s + D\partial_\tau)\right)\sum_{k=1}^{n}\epsilon^k \mathbf{u}_k =$$

$$\left(u_{3,0}M\mathbf{u}_0 + \sum_{k=1}^{n}\epsilon^k(\sum_{l=1}^{k-1}u_{3,k-l}M\mathbf{u}_l) + \sum_{k=1}^{n}\epsilon^k J_0\mathbf{u}_k\right)(Gr_h + j\epsilon^2).$$

The operators at each order are

$$L_0 = \omega_0 D\partial_s - I\nabla^2 - A$$

$$L_1 = \omega_1 D\partial_s$$

$$L_2 = \omega_2 D\partial_s + D\partial_\tau.$$

$$L_3 = \omega_3 D\partial_s + \omega_1 D\partial_\tau.$$

The systems at each order are:

- $O(\epsilon^0)$:

$$L_0\mathbf{u}_0 = Gr_h u_{3,0}M\mathbf{u}_0$$

- $O(\epsilon)$:

$$(L_0 - Gr_h J_0)\mathbf{u}_1 = -L_1\mathbf{u}_0$$

- $O(\epsilon^2)$:

$$(L_0 - Gr_h J_0)\mathbf{u}_2 = -L_1\mathbf{u}_1 - L_2\mathbf{u}_0 + Gr_h u_{3,1}M\mathbf{u}_1 + ju_{3,0}M\mathbf{u}_0$$

- $O(\epsilon^3)$:

$$(L_0 - Gr_h J_0)\mathbf{u}_3 = -L_3\mathbf{u}_0 - L_1\mathbf{u}_2 - L_2\mathbf{u}_1 + Gr_h u_{3,2}M\mathbf{u}_1 + Gr_h u_{3,1}M\mathbf{u}_2 + jJ_0\mathbf{u}_1.$$

We now outline the steps in the asymptotic analysis. Compute $\mathbf{u}_0$ by solving the steady-state equations to get a solution $\mathbf{u}_0(r)$. Because $\mathbf{u}_0$ is independent of time $L_1\mathbf{u}_0 = L_2\mathbf{u}_0 = L_3\mathbf{u}_0 = 0$.

At order ϵ,

$$(L_0 - Gr_h J_0)\mathbf{u}_1 = 0.$$

Compute $\mathbf{u}_1$ by solving the eigenvalue problem to get

$$\mathbf{u}_1 = a(\tau)\mathbf{A}(r)e^{is} + \bar{a}(\tau)\bar{\mathbf{A}}(r)e^{-is}$$

and ω_0.

At order ϵ^2,

$$(L_0 - Gr_h J_0)\mathbf{u}_2 = -L_1\mathbf{u}_1 + Gr_h u_{3,1}M\mathbf{u}_1 + ju_{3,0}M\mathbf{u}_0.$$

The term $L_1\mathbf{u}_1$ will produce expressions in e^{is}, which are resonant terms. Then to suppress these resonant terms choose $\omega_1 = 0$. The other terms on the right hand side will produce expressions in e^0, e^{2is}, and e^{-2is}, so compute the solution $\mathbf{u}_2$ using the method of undetermined coefficients, by solving a system $Lu = b$ for each of the harmonic terms.

Formulate the $O(\epsilon^3)$ problem and use Fredholm's Alternative Theorem to find a solvability condition. We now proceed with a discussion of the analysis as outlined.

C.4. *Steady State Problem*

This solution was discussed in section C.1:

$$\mathbf{u}_0 = \begin{pmatrix} u_{10} \\ u_{20} \\ u_{30} \end{pmatrix}.$$

C.5. *Linear Problem*

This solution was discussed in section C.2:

$$\mathbf{u}_1 = \begin{pmatrix} u_{11} \\ u_{21} \\ u_{31} \end{pmatrix} = a(\tau)\mathbf{A}_1(r)e^{is} + \bar{a}(\tau)\bar{\mathbf{A}}_1(r)e^{-is}.$$

C.6. *Second Order Problem*

At order ϵ^2, the right hand side is

$$ju_{30}M\mathbf{u}_0 + Gr_h u_{31}M\mathbf{u}_1.$$

Examine each term. First,

$$ju_{30}M\mathbf{u}_0 = j\begin{pmatrix} u_{30}u_{20} \\ -u_{30}u_{10} \\ 0 \end{pmatrix}$$

which is known from the order ϵ^0 equation. Second,

$$\begin{aligned} Gr_h u_{31}M\mathbf{u}_1 &= Gr_h(aA_{31}e^{is} + \bar{a}\bar{A}_{31}e^{-is})M(a\mathbf{A}_1 e^{is} + \bar{a}\bar{\mathbf{A}}_1 e^{-is}) \\ &= 2a\bar{a}Gr_h\begin{pmatrix} A_{31}\bar{A}_{21} \\ -A_{31}\bar{A}_{11} \\ 0 \end{pmatrix} + a^2 Gr_h\begin{pmatrix} A_{31}A_{21} \\ -A_{31}A_{11} \\ 0 \end{pmatrix}e^{2is} \\ &\quad + \bar{a}^2 Gr_h\begin{pmatrix} \bar{A}_{31}\bar{A}_{21} \\ -\bar{A}_{31}\bar{A}_{11} \\ 0 \end{pmatrix}e^{-2is}, \end{aligned}$$

so the right hand side is

$$\begin{aligned} &j\begin{pmatrix} u_{30}u_{20} \\ -u_{30}u_{10} \\ 0 \end{pmatrix} + 2|a|^2 Gr_h Real\left(\begin{pmatrix} A_{31}\bar{A}_{21} \\ -A_{31}\bar{A}_{11} \\ 0 \end{pmatrix}\right) \\ &+ a^2 Gr_h\begin{pmatrix} A_{31}A_{21} \\ -A_{31}A_{11} \\ 0 \end{pmatrix}e^{2is} + \bar{a}^2 Gr_h\begin{pmatrix} \bar{A}_{31}\bar{A}_{21} \\ -\bar{A}_{31}\bar{A}_{11} \\ 0 \end{pmatrix}e^{-2is}. \end{aligned}$$

Solving with this right hand side leads to a solution

$$\mathbf{u}_2 = \begin{pmatrix} u_{12} \\ u_{22} \\ u_{32} \end{pmatrix} = \mathbf{B}_0(r) + (a^2\mathbf{B}_2(r)e^{2is} + c.c.),$$

where

$$\mathbf{B}_0 = j\mathbf{b}_0^{(1)}(r) + |a|^2\mathbf{b}_0^{(2)}(r)$$

is the solution of a real operator with a real right hand side, and so is real.

C.7. *The Landau Equation*

Apply Fredholm's alternative at order ϵ^3; adopting the notation used in Joseph Joseph(1976)

$$\langle \mathbf{a} \cdot \bar{\mathbf{b}} \rangle = \int_{\mathcal{V}} \mathbf{a} \cdot \bar{\mathbf{b}} d\mathcal{V}$$

$$[\mathbf{a}, \mathbf{b}] = \frac{1}{T} \int_0^T \langle \mathbf{a} \cdot \bar{\mathbf{b}} \rangle dt.$$

Solve the adjoint homogeneous problem,

$$(L_0 - Gr_h J_0)^* \mathbf{z} = 0$$

and then require for solvability that $\mathbf{f}$, the right hand side at order ϵ^3, satisfies

$$[\mathbf{f}, \mathbf{z}] = 0.$$

The order ϵ^3 right hand side is

$$-L_2 \mathbf{u}_1 + Gr_h u_{32} M \mathbf{u}_1 + Gr_h u_{31} M \mathbf{u}_2 + j J_0 \mathbf{u}_1.$$

Examine each term. First,

$$\begin{aligned} -L_2 \mathbf{u}_1 &= -(\omega_2 D\partial_s + D\partial_\tau) \left[a\mathbf{A}_1 e^{is} + \bar{a}\bar{\mathbf{A}}_1 e^{-is} \right] \\ &= -\omega_2 D[ai\mathbf{A}_1 e^{is} - \bar{a}i\bar{\mathbf{A}}_1 e^{-is}] - [\frac{da}{d\tau} D\mathbf{A}_1 e^{is} + \frac{d\bar{a}}{d\tau} D\bar{\mathbf{A}}_1 e^{-is}]. \end{aligned}$$

Second,

$$\begin{aligned} Gr_h u_{32} M \mathbf{u}_1 &= Gr_h (B_{30} + a^2 B_{32} e^{2is} + \bar{a}^2 \bar{B}_{32} e^{-2is}) M (a\mathbf{A}_1 e^{is} + \bar{a}\bar{\mathbf{A}}_1 e^{-is}) \\ &= Gr_h \begin{pmatrix} jb_{30}^{(1)}(aA_{21}e^{is}) + b_{30}^{(2)}(a^2\bar{a}A_{21}e^{is}) + (a^2\bar{a}B_{32}\bar{A}_{21}e^{is}) \\ -j\left(b_{30}^{(1)}(aA_{11}e^{is}) + b_{30}^{(2)}(a^2\bar{a}A_{11}e^{is}) + (a^2\bar{a}B_{32}\bar{A}_{11}e^{is})\right) \\ 0 \end{pmatrix} + c.c. \end{aligned}$$

Third,

$$\begin{aligned} Gr_h u_{31} M \mathbf{u}_2 &= Gr_h \left(aA_{31}e^{is}) M(j\mathbf{b}_0^{(1)} + |a|^2 \mathbf{b}_0^{(2)} + a^2 \mathbf{B}_2 e^{2is} \right) \\ &= Gr_h \begin{pmatrix} jb_{20}^{(1)}(aA_{31}e^{is}) + b_{20}^{(2)}(a^2\bar{a}A_3 1e^{is}) + j(a^2\bar{a}B_{22}\bar{A}_{31}e^{is}) \\ b_{10}^{(1)}(aA_{31}e^{is}) + b_{10}^{(2)}(a^2\bar{a}A_3 1e^{is}) + (a^2\bar{a}B_{12}\bar{A}_{31}e^{is}) \\ 0 \end{pmatrix} + c.c. \end{aligned}$$

Lastly,

$$jJ_0 \mathbf{u}_1 = ja \begin{pmatrix} u_{30}A_{21} + u_{20}A_{31} \\ -u_{30}A_{11} - u_{10}A_{31} \\ 0 \end{pmatrix} e^{is} + c.c.$$

So the right hand side is

$$
\begin{aligned}
&-\omega_2 D[ai\mathbf{A}_1 e^{is} + c.c.] - [\frac{da}{d\tau} D\mathbf{A}_1 e^{is} + c.c.] \\
&+ Gr_h \begin{pmatrix} jb_{30}^{(1)}(aA_{21}e^{is}) + jb_{30}^{(2)}(a^2\bar{a}A_{21}e^{is}) + (a^2\bar{a}B_{32}\bar{A}_{21}e^{is}) \\ -\left(b_{30}^{(1)}(aA_{11}e^{is}) + b_{30}^{(2)}(a^2\bar{a}A_{11}e^{is}.) + (a^2\bar{a}B_{32}\bar{A}_{11}e^{is})\right) \\ 0 \end{pmatrix} + c.c. \\
&+ Gr_h \begin{pmatrix} jb_{20}^{(1)}(aA_{31}e^{is}) + jb_{20}^{(2)}(a^2\bar{a}A_31e^{is}) + (a^2\bar{a}B_{22}\bar{A}_{31}e^{is}) \\ b_{10}^{(1)}(aA_{31}e^{is}) + b_{10}^{(2)}(a^2\bar{a}A_31e^{is}) + (a^2\bar{a}B_{12}\bar{A}_{31}e^{is}) \\ 0 \end{pmatrix} + c.c. \\
&+ ja \begin{pmatrix} u_{30}A_{21} + u_{20}A_{31} \\ -u_{30}A_{11} - u_{10}A_{31} \\ 0 \end{pmatrix} e^{is} + c.c.
\end{aligned}
$$

Now enforce

$$[\mathbf{f}, \mathbf{z}] = 0.$$

Compute the time integral of this solvability condition first; then the only non-zero components are constant in time (s). These terms are

$$
\begin{aligned}
&-\omega_2 Dai\mathbf{A}_1 \cdot \bar{\mathbf{z}} - \frac{da}{d\tau} D\mathbf{A}_1 \cdot \bar{\mathbf{z}} + jGr_h a \begin{pmatrix} b_{30}^{(1)}A_{21} \\ b_{30}^{(1)}A_{11} \\ 0 \end{pmatrix} \cdot \bar{\mathbf{z}} + jGr_h a \begin{pmatrix} b_{20}^{(1)}A_{31} \\ b_{10}^{(1)}A_{31} \\ 0 \end{pmatrix} \cdot \bar{\mathbf{z}} \\
&+ ja \begin{pmatrix} u_{30}A_{21} + u_{20}A_{31} \\ -u_{30}A_{11} - u_{10}A_{31} \\ 0 \end{pmatrix} \bar{\mathbf{z}} + Gr_h a^2\bar{a} \begin{pmatrix} b_{30}^{(2)}A_{21} \\ b_{30}^{(2)}A_{11} \\ 0 \end{pmatrix} \cdot \bar{\mathbf{z}} \\
&+ Gr_h a^2\bar{a} \begin{pmatrix} b_{20}^{(2)}A_{31} \\ b_{10}^{(2)}A_{31} \\ 0 \end{pmatrix} \cdot \bar{\mathbf{z}} + Gr_h a^2\bar{a} \begin{pmatrix} B_{32}\bar{A}_{21} + B_{22}\bar{A}_{31} \\ B_{32}\bar{A}_{11} + B_{12}\bar{A}_{31} \\ 0 \end{pmatrix} \cdot \bar{\mathbf{z}}.
\end{aligned}
$$

Now compute the volume integral of these terms and set it to zero, arriving at an ODE in a:

$$\alpha_0 \frac{da}{d\tau} = j\alpha a + \beta a|a|^2 \tag{C 1}$$

where the coefficients α_0, α and β are determined via the volume integral.

The nature of the bifurcation has been reduced to the study of an ODE. Here is the Hopf bifurcation theorem as stated in Glendinning Glendinning(1994):

Theorem C.1 *(Hopf Bifurcation Theorem, Subcritical Case)*
Suppose that $\dot{x} = f(x, y, \mu)$, $\dot{y} = g(x, y, \mu)$ with $f(0, 0, \mu) = g(0, 0, \mu) = 0$ and that the Jacobian matrix evaluated at the origin when $\mu = 0$ is

$$\begin{pmatrix} 0 & -\omega \\ \omega & 0 \end{pmatrix}$$

for some $\omega \neq 0$. If $f_{\mu x} + g_{\mu y} \neq 0$ and $c \neq 0$ then a curve of periodic solutions bifurcates from the origin into $\mu < 0$ if $c(f_{mux} + g_{\mu y}) > 0$. If $f_{\mu x} + g_{\mu y} > 0$, then the origin is stable for $\mu < 0$ and unstable for $\mu > 0$. If the origin is stable on the side of $\mu = 0$ for which the periodic solutions exist, the periodic solutions are unstable and the bifurcation

is subcritical. The constant c is given by

$$c = \frac{1}{16}(f_{xxx} + g_{xxy} + f_{xyy} + g_{yyy}) +$$

$$\frac{1}{16\omega}(f_{xy}(f_{xx} + f_{yy}) - g_{xy}(g_{xx} + g_{yy}) - f_{xx}g_{xx} + f_{yy}g_{yy})$$

evaluated at $(x, y) = (0, 0)$.

This theorem can be applied as follows. Rescale the equation C 1 to get

$$\frac{da}{d\tau} = j\alpha a + \beta|a|^2 a$$

Then breaking the system into its real and imaginary parts, the system is in the form in the theorem as stated above. The requirements for a subcritical bifurcation are met when $j = -1$ and $\alpha_r < 0, \beta_r > 0$. The computation of these coefficients is straightforward and is being undertaken at this time. At the end of this chapter we will explain a method of approximating these coefficients as an alternative to computing them directly. Now we turn to an examination of the Hopf bifurcation in the Lorenz equations.

Appendix D. Chebyshev Polynomials

REFERENCES

Ascher, U. M., Ruuth, S. J. & Wetton, B. T. 1995 Implicit-explicit methods for time-dependent partial differential equations. *SIAM Journal on Numerical Analysis* **32**, 797–823.

Bergeron, K., Coutsias, E. A., Lynov, J. P. & Nielsen, A. H. 2000 Dynamical properties of forced shear layers in an annular geometry. *Journal of Fluid Mechanics* **402**, 255–289.

Burroughs, E., Romero, L., Lehoucq, R. & Salinger, A. submitted 2002 Linear stability of flow in a differentially heated cavity via large-scale eigenvalue calculations. *International Journal of Numerical Methods in Heat and Fluid Flow* .

Burroughs, E. A., Romero, L. A., Lehoucq, R. B. & Salinger, A. G. 2001 Large scale eigenvalue calculations for computing the stability of buoyancy driven flows. Technical Report SAND2001–0113. Sandia National Laboratories, Albuquerque, NM.

Canuto, C., Hussaini, M., Quarteroni, A. & Zang, T. 1988 *Spectral Methods in Fluid Dynamics*. New York: Springer-Verlag.

Coutsias, E. A., Hagstrom, T., Hesthaven, J. & Torres, D. C. 1995 Integration preconditioners for differential operators in spectral tau-methods. In *ICOSAHOM-95. Proceedings. 3. International conference on spectral and high order methods* (ed. L. Ilin, A.V.; Ridgway Scott), pp. 21—38. Houston Journal of Mathematics.

Fornberg, B. 1998 *A Practical Guide to Pseudospectral Methods*. New York: Cambridge University Press.

Gelfand, I. M. & Fomin, S. V. 1991 *Calculus of Variations*. New York: Dover.

Glendinning, P. 1994 *Stability, instability and chaos: an introduction to the theory of nonlinear differential equations*. New York: Cambridge University Press.

Gottlieb, D. & Orszag, S. A. 1977 *Numerical Analysis of Spectral Methods: Theory and Applications*. Philadelphia: SIAM.

Hendrickson, B. & Leland, R. 1995 The Chaco user's guide: Version 2.0. *Tech. Rep.* SAND94–2692. Sandia National Labs, Albuquerque, NM.

Hughes, T. J. R., Franca, L. P. & Hulbert, G. M. 1989 A new finite element formulation for computational fluid dynamics: VIII. the Galerkin/least-squares method for advective-diffusive equations. *Computational Methods Applied Mechanics and Engineering* **73**, 173–189.

JAPIKSE, D. 1973 Advances in thermosyphon technology. In *Advances in Heat Transfer* (ed. T.F.Irvine & J. Hartnett), , vol. 9, pp. 1–111. New York: Academic Press.

JOSEPH, D. D. 1976 *Stability of Fluid Motions I*. New York: Springer-Verlag.

KEENER, J. P. 1995 *Principles of Applied Mathematics*. Reading, Massachusetts: Perseus Books.

KELLER, J. B. 1966 Periodic oscillations in a model of thermal convection. *Journal of Fluid Mechanics* **26(3)**, 599–606.

LANDAU, L. D. & LIFSHITZ, E. M. 1999 *Fluid Mechanics, 2nd Edition: Course of Theoretical Physics, Vol. 6*. Boston, MA: Butterworth-Heineman.

LEHOUCQ, R. & SALINGER, A. 2001 Large-scale eigenvalue calculations for stability analysis of steady flows on massively parallel computers. *International Journal of Numerical Methods in Fluids* **36**, 309–327.

LORENZ, E. N. 1963 Deterministic nonperiodic flow. *Journal of the Atmospheric Sciences* **20**, 130–141.

RODRÍGUEZ-BERNAL, A. & VAN VLECK, E. S. 1998 Diffusion induced chaos in a closed loop thermosyphon. *SIAM J. Appl. Math* **58(4)**, 1072–1093.

SALINGER, A. G., DEVINE, K. D., HENNIGAN, G. L., HUTCHINSON, S. A., MOFFAT, H. K. & SHADID, J. N. 1999 MPSalsa: a finite element computer program for reacting flow problems Part 2. User's guide. Technical Report SAND96–2331. Sandia National Laboratories, Albuquerque, NM.

SALINGER, A. G., DEVINE, K. D., HENNIGAN, G. L., MOFFAT, H. K., HUTCHINSON, S. A. & SHADID, J. N. 1996 MPSalsa: a finite element computer program for reacting flow problems Part 1. User's guide. Technical Report SAND95–2331. Sandia National Laboratories, Albuquerque, NM.

SHADID, J. 1999 A fully-coupled Newton-Krylov solution method for parallel unstructured finite element fluid flow, heat and mass transport. *IJCFD* **12**, 199–211.

SHADID, J., TUMINARO, R. & WALKER, H. 1997 An inexact Newton method for fully coupled solution of the Navier-Stokes equations with heat and mass transport. *Journal of Computational Physics* **137**, 155–185.

SHADID, J. N., SALINGER, A. G., SCHMIDT, R., SMITH, T. M., HUTCHINSON, S. A., HENNIGAN, G. L., DEVINE, K. D. & MOFFAT, H. 1999 MPSalsa version 1.5, a finite element computer program for reacting flow problems Part 1: Theoretical development. Technical Report SAND98–2864. Sandia National Laboratories, Albuquerque, NM.

TORRANCE, K. 1979 Open-loop thermosyphons with geological applications. *Journal of Heat Transfer* **101**, 677–683.

TRITTON, D. 1988 *Physical Fluid Dynamics*. Oxford: Clarendon Press.

TUMINARO, R. S., HEROUX, M., HUTCHINSON, S. A. & SHADID, J. N. 1999 Aztec user's guide: Version 2.1. Technical Report SAND99-8801J. Sandia National Laboratories, Albuquerque, NM.

VELÁZQUEZ, J. J. L. 1994 On the dynamics of a closed thermosyphon. *SIAM J. Appl. Math* **54:6**, 1561–1593.

WELANDER, P. 1967 On the oscillatory instability of a differentially heated fluid loop. *Journal of Fluid Mechanics* **29(1)**, 17–30.

YUEN, P. K. & BAU, H. H. 1996 Rendering a subcritical Hopf bifurcation supercritical. *Journal of Fluid Mechanics* **317**, 91–109.